UNITED NATIONS EDUCATIONAL, SCIENTIFIC AND CULTURAL ORGANIZATION
INTERNATIONAL ATOMIC ENERGY AGENCY
INTERNATIONAL CENTRE FOR THEORETICAL PHYSICS
I.C.T.P., P.O. BOX 586, 34100 TRIESTE, ITALY, CABLE: CENTRATOM TRIESTE

SMR/930 - 20

"Workshop on El Niño, Southern Oscillation and Monsoon"
15 - 26 July 1996

"Seasonal & Interannual Variability of Atmospheric Heat Sources"

M. YANAI
University of California - Los Angeles
USA

Please note: These are preliminary notes intended for internal distribution only.

Seasonal and Interannual Variability of Atmospheric Heat Sources

MICHIO YANAI AND TOMOHIKO TOMITA

Department of Atmospheric Sciences, University of California, Los Angeles
405 Hilgard Avenue, Los Angeles, CA 90095-1565, U.S.A

ABSTRACT

Using the NCEP/NCAR reanalysis (Kalnay et al. 1996), global distributions of the heat source Q_1 and moisture sink Q_2 are determined for a 15-year period from 1980 to 1994. In northern winter, the major heat sources are located (i) in a broad zone connecting the equatorial Indian Ocean, Indonesia and the South Pacific Convergence Zone (SPCZ), (ii) over the Congo and Amazon Basins, and (iii) off the east coasts of Asia and North America. In northern summer, the major heat sources are over (i) the Bay of Bengal coast, (ii) the western tropical Pacific, and (iii) Central America. Throughout the year, the South Indian Ocean, eastern parts of the North and South Pacific Ocean, and eastern parts of the North and South Atlantic Ocean remain to be heat sinks.

Heating mechanisms operating in various parts of the world are examined by comparing the horizontal distributions of the vertically integrated heat source $<Q_1>$ with those of the vertically integrated moisture sink $<Q_2>$ and outgoing longwave radiation (OLR) flux, and by comparing the vertical profiles of Q_1 with those of Q_2. Over the tropical oceans, heat released by condensation with deep cumulus convection provides the major heat source. The radiative cooling and moistening due to evaporation are dominant features over the subtropical oceans where subsidence prevails. The desert regions of Sahara and Australia are characterized by large sensible heating near the surface and intense radiative cooling aloft. Over the Tibetan Plateau the profiles of Q_1 and Q_2 show the importance of sensible heating in spring and contributions from the release of latent heat of condensation in summer.

Heat sources in various regions exhibit strong interannual variability. A long (4-5 years) periodicity corresponding to the variation of SST is evident over the equatorial central and eastern Pacific, while a quasi-biennial oscillation is seen over the equatorial Indian Ocean. Examples of anomalous heating distributions during the 1986/88 ENSO event and year to year variations of heating over the Tibetan Plateau are discussed.

1. Introduction

Since the First Global Atmosphere Research Program (GARP) Global Experiment (FGGE) (December 1978 - November 1979), many attempts have been made to determine global distributions of atmospheric heat sources and sinks. Wei et al. (1983), Johnson et al. (1987) and Schaack et al. (1990) estimated the seasonal global distributions of the mean tropospheric heating rate through vertical integration of the isentropic mass continuity equation, using the National Meteorological Center (NMC) FGGE III-a and European Centre for Medium-Range Weather Forecasts (ECMWF) FGGE III-b analyses. They showed that the major heat sources are located over South America, equatorial Africa, the intertropical convergence zone (ITCZ), the Asian monsoon circulation and the oceanic cyclone tracks of the Northern Hemisphere (NH) and that the primary centers of heating migrate meridionally and zonally with the annual variations of the latitude of maximum incoming solar radiation and the planetary scale land-sea thermal contrast. Schaack et al. (1990) examined also the vertical profiles of the monthly mean heating rates for various geographical regions.

Hoskins et al. (1989) estimated the global-scale atmospheric heat sources and sinks based on the initialized ECMWF/ World Meteorological Organization (WMO) analyses from 1979 to 1989. They showed large seasonal and interannual variability of atmospheric heating during these years. Christy (1991), using the ECMWF analyses from May 1985 to December 1987, calculated vertically integrated diabatic heating rates as residuals of the thermodynamic budget. Trenberth and Solomon (1994) discussed the global heat balane using the top-of-the atmosphere radiation from the Earth Radiation Budget Experiment with the ECMWF data for each month of 1988. Schaack and Johnson (1994), utilizing the uninitialized ECMWF/Tropical Oceans Global Atmosphere (TOGA) analyses, estimated three-dimensional global distributions of atmospheric heating for January and July of the 3-year period 1986-88, a period that included an El Nino - Southern Oscillation (ENSO) cycle. Their results show that large fluctuations in the magnitude of heating and the disposition of maxima/minima in the tropics occurred over the 3-year period. The vertical

distributions of heating rate for selected regions also revealed large interannual variability.

On regional scale, many authors have studied the heat sources and moisture sinks as residuals of the heat and moisture budgets over the Tibetan Plateau and surrounding areas using FGGE II-b and the Chinese Qinghai-Xizang Plateau Meteorology Experiment (QXPMEX) data (e.g., Nitta 1983; Luo and Yanai 1984; He et al. 1987; Yanai et al. 1992; Yanai and Li 1994a). Their results showed that the structure and time evolution of the Asian summer monsoon circulations are closely related to the horizontal and vertical distributions of atmospheric heating over the Tibetan Plateau and its vicinity. Li and Yanai (1996) discussed the importance of warming of the air above the Eurasian continent centered on the Tibetan Plateau and the resulting reversal of the meridional temperature gradient for the onset of the Asian summer monsoon.

Li and Yanai (1996) also examined the global distributions of heat source and moisture sink of the troposphere using the ECMWF/TOGA analyses from 1985 to 1992. They found that strong Asian summer monsoon as defined by Webster and Yang (1992) is associated with enhanced heating over the Arabian Sea, the Bay of Bengal and the western Pacific Ocean, and reduced heating over the equatorial Indian Ocean and the central and eastern Pacific. In the year of weak Asian summer monsoon, the heating over South Asia is significantly weakened, while heating over the equatorial central Pacific to the coast of South America is remarkably enhanced.

As discussed by several authors (e.g., Trenberth and Olson 1988; Hoskins et al. 1989; Schaack and Johnson 1994), however, the continuity of the ECMWF analyses was impacted by the changes routinely made to assimilation system for the purpose of improving numerical weather predicton. During the period from 1985 to 1992, several changes in the ECMWF analysis/forecast scheme were made (e.g., Trenberth 1992). The changes in scheme made during this period may have impact on the analyses and consequently the derived fields such as heating and drying rates. Although Yanai and Li (1996) found no obvious evidence of discontinuities in time series of these quantities during this period, the impact of these changes on the analyses is difficult to estimate.

Recently, the National Centers for Environmental Prediction (NCEP) and National Center for Atmospheric Research (NCAR) released the global analyses from 1980 to 1994 as part of their 40-year Reanalysis Project. The NCEP/NCAR reanalysis uses a frozon global data assimilation system and a database as complete as possible (Kalnay et al. 1996).

The purpose of this paper is to revise and extend the results of Li and Yanai (1996) using the NCEP/NCAR reanalysis from 1980 to 1994. We examine in detail the seasonal and interannual variability of heat sources and sinks and the mechanisms of heating over various geographical regions. In section 2 we discuss the data and analysis procedures of the current work. Section 3 describes the horizontal distributions and seasonal variations of the vertically integrated heat sources and sinks. In section 4 we examine the vertical profiles of heat sources and moisture sinks for various geographycal regions to identify the regional characteristics of heating mechanisms. Section 5 illustrates of interannual variations of heat sources and sinks. Anomalous heating distributions during the 1986/88 ENSO event, and interannual variations of heating over the Tibetan Plateau are illustrated. The summary and discussions are given in section 6.

2. Data and analysis procedures

The major data used in this work are the twice daily (0000 and 1200 UTC) NCEP/NCAR reanalyses on a $2.5^0 \times 2.5^0$ grid for the domain 50^oS - 50^oN; 0^o - 360^o from 1980 to 1994. Zonal and meridional wind components and temperature are given at 17 standard pressure levels (1000, 925, 850, 700, 600, 500, 400, 300, 250, 200, 150, 100, 70, 50, 30, 20, and 10 hPa). Relative humidity are given at 8 levels. The NCEP/NCAR reanalysis provides also the pressures at the surface and the tropopause. The outgoing longwave radiation (OLR) flux and the NCEP Climate Analysis Center (CAC) sea surface temperature (SST) are also used in this work.

The apparent heat source Q_1 and the apparent moisture sink Q_2 (e.g., Yanai et al. 1973; Yanai and Johnson 1993) are computed from

$$Q_1 = C_p \left(\frac{p}{p_0}\right)^{\kappa} \left(\frac{\partial \theta}{\partial t} + V \cdot \nabla \theta + \omega \frac{\partial \theta}{\partial p}\right), \tag{1}$$

$$Q_2 = -L \left(\frac{\partial q}{\partial t} + V \cdot \nabla q + \omega \frac{\partial q}{\partial p}\right). \tag{2}$$

In (1) and (2), θ is the potential temperature, q the mixing ratio of water vapor, V the horivontal velocity, ω the vertical p-velocity, p the pressure. $\kappa = R/C_p$, R and C_p are respectively the gas constant and the specific heat at constant pressure of dry air, $p_0 = 1000$ hPa and L the latent heat of condensation. ∇ is the isobaric gradient operator.

The vertical p-velocity ω is recalculated from the horizontal divergence by vertically integrating the continuity equation

$$\frac{1}{a\cos\phi}\left[\frac{\partial u}{\partial \lambda} + \frac{\partial}{\partial \phi}(v\cos\phi)\right] + \frac{\partial \omega}{\partial p} = 0, \tag{3}$$

with the surface boundary condition

$$\omega = \omega_s = -g\rho_s \left(\frac{u_s}{a\cos\phi}\frac{\partial h}{\partial \lambda} + \frac{v_s}{a}\frac{\partial h}{\partial \phi}\right) \qquad \text{at } p = p_s. \tag{4}$$

In (3) and (4) u and v are the zonal and meridional components of the horizontal wind, a the mean earth radius, λ the longitude, ϕ the latitude, g the acceleration of gravity, ρ the air density, and h the terrain height. The suffix s denotes the surface value. The values of smoothed terrain height on a $2.5^0 \times 2.5^0$ mesh are taken from the NMC global elevation data.

To obtain reliable estimates of Q_1 and Q_2 especially Q_1 in the upper troposphere where the static stability is high, we need accurate estimates of ω to be used in (1) and (2). Above the tropopause where the convective heat transport vanishes, we may set

$$Q_1 = Q_R \tag{5}$$

where Q_R is the radiative heating rate. Nitta (1977) assumed (5) at $p = p_T$ where p_T is the tropopause pressure. In this study we impose the adiabatic condition

$$\omega = \omega_T = -\left(\frac{\partial \theta}{\partial t} + V \cdot \nabla \theta\right) \Big/ \left(\frac{\partial \theta}{\partial p}\right) \qquad \text{at } p = p_T, \tag{5a}$$

for simplicity. This was justified by an empirical fact that Q_R is small near the tropopause (e. g., Dopplick 1979). The original estimates of the horizontal divergence, D_0, are adjusted by adding

$$D' = \left(\omega_T - \omega_s - \int_{p_T}^{p_s} D_0 \, dp\right) \Big/ (p_s - p_T). \tag{6}$$

Then the corrected divergence, $D = D_0 + D'$, is used in (3) to obtain the adjusted values of D and ω at all levels.

Q_1 and Q_2 are calculated for the layer between the ground surface and the first standard pressure level above the surface, and for each successive layer between the standard pressure levels. Because of the horizontally varying terrain height and tropopause pressure, the number of layers for which Q_1 and Q_2 values are obtained may vary from a grid point to the next. To obtain reliable estimates of Q_1 and Q_2 from (1) and (2), we design the finite difference forms for the horizontal and vertical advection terms to maintain their consistency with their flux forms accurately. The advection terms are evaluated at every observation time and the (1, 2, 1) weighted average over three observation times is made to define mean Q_1 and Q_2 values over 24 hours. The local time change terms are evaluated using the centered difference of θ and q over 24 hours.

As discussed by Yanai et al. (1973), Q_1 and Q_2 are the residuals of heat and moisture budgets of the resolvable motion and may be interpreted as

$$Q_1 = Q_R + L(c - e) - \frac{\partial}{\partial p}\overline{s'\omega'}, \tag{7}$$

$$Q_2 = L(c - e) + L\frac{\partial}{\partial p}\overline{q'\omega'}, \tag{8}$$

where c is the rate of condensation per unit mass of air. e is the rate of re-evaporation of cloud water. $s = C_p T + gz$ is the dry static energy. T is the temperature. The prime denotes the deviation from the average due to unresolved eddies such as cumulus convection and turbulence. The eddy vertical flux terms may have significant contributions to Q_1 and Q_2 in highly convective situations. From (7) and (8) we find

$$Q_1 - Q_2 - Q_R = -\frac{\partial}{\partial p}\overline{(s' + Lq')\omega'}. \tag{9}$$

(9) has been widely used to measure the activity of cumulus convection (e.g., Yanai et al. 1973; Yanai and Johnson 1993).

Integrating (7) and (8) from the tropopause pressure p_T to the surface pressure p_s, we obtain

$$\langle Q_1 \rangle = \langle Q_R \rangle + LP + S, \tag{10}$$

$$\langle Q_2 \rangle = L(P - E), \tag{11}$$

where

$$\langle\ \rangle = \frac{1}{g}\int_{p_T}^{p_s}(\ )dp. \tag{12}$$

P, S and E are the precipitation rate, the sensible heat flux, and the evaporation rate, respectively, per unit area at the surface.

Equations (7) - (11) are useful for the physical interpretation of the budget results. First, the relations (10) and (11), with the distribution of OLR, serve to verify the accuracy and mutual consistency of the estimates of Q_1 and Q_2. If the heating over a certain area is primarily due to the condensation process, the values of $<Q_1>$ and $<Q_2>$ should be similar to each other and the OLR may have a small value. On the other hand, the presence of strong sensible heat flux or evaporation from the surface may cause significant difference between the horizontal distributions of $<Q_1>$ and $<Q_2>$.

Second, the comparison between the vertical distributions of Q_1 and Q_2 serves to find the presence or absence of eddy vertical transport process. If the heating is mainly due to the condensation associated with stratiform clouds, the vertical profiles of Q_1 and Q_2 will be very similar. On the other hand, if the release of latent heat is associated with cumulus convection, the profiles of Q_1 and Q_2 will differ from each other and there will be a separation in the levels of peak values of Q_1 and Q_2 because of the presence of eddy vertical transport process (e.g., Yanai et al. 1973; Thompson et al. 1979). If the heating is due to the supply of sensible heat flux from the dry ground surface, we expect to obtain the heat source that does not accompany the moisture sink. In such a situation the vertical profiles of Q_1 will be determined by the redistribution process due to turbulence or dry thermal convection.

Figure 1a shows the time series of the monthly mean vertically integrated heat source $<Q_1>$ and moisture sink $<Q_2>$ from 1980 to 1994, averaged over the area 85^0E-105^0E, 5^0-25^0N, where the maximum heating occurs in summer (see Fig. 4a). Figure 1b shows the time series of the monthly zonal wind component from 1985 to 1992 averaged over the same area where the southwesterlies at lower levels and the northeasterlies at upper levels dominate in summer and the flows reverse their directions in winter.

3. Horizontal distributions of heat sources and moisture sinks

The 15-year mean horizontal distributions of the vertically integrated heat source $<Q_1>$ and moisture sink $<Q_2>$, and OLR flux for northern winter (December - February) are shown together in Fig. 2. During northern winter the major heat sources ($\geq$ 100 Wm^{-2}) are found along the North Pacific and North Atlantic storm tracks, and over the southern Africa, South America and the region spanning from the South Indian Ocean through the Indonesian maritime continent to the South Pacific convergence zone (SPCZ) (Fig. 2a). Cooling is found over the NH continents and eastern parts of the subtropical oceans. The heat sources in the tropics are accompanied by moisture sink $<Q_2>$ of similar magnitude (Fig. 2b), indicating that condensational heating is the major component of heat sources. On the other hand, the heat sources along the North Pacific and North Atlantic storm tracks are

accompanied by very small values of $<Q_2>$, suggesting the dominant role of sensible heat flux from the warm ocean surface. In the oceanic subtropical latitudes, large negative values of $<Q_1>$ and $<Q_2>$ (~ -100 Wm^{-2}) indicate strong radiative cooling exceeding sensible and latent heating [see (10)] and strong evaporation exceeding precipitation [see (11)]. The distributions of large $<Q_1>$ and $<Q_2>$ in the tropics are in remarkable agreement with the distribution of the OLR flux less than 240 Wm^{-2}, showing that the heating is associated with deep cumulus convection.

In northern spring (March - May), much of the Asian and North American land masses becomes heat sources (Fig. 3a). Comparison with small values of $<Q_2>$ over the continents (Fig. 3b) suggests that sensible heat flux from ground surface is the major component of heat sources (Li and Yanai 1996). The heat sources along the North Pacific and North Atlantic storm tracks are drastically weakened. The heat sources in the tropics have moved northward and are centered over the equator. Comparisons with the values of $<Q_2>$ and OLR flux (Fig. 3c) indicate that the northward displacement of the tropical heating is the consequence of the northward movement of the major convective rainbelt in the tropics. Compared with the other seasons, both convection and heating in the tropics are least vigorous in spring.

In northern summer (June - August), the major heat sources in the tropics are located to the north of the equator (Fig. 4a). Both heating and convection become most robust. Principal heat sources are located over the region of the Asian summer monsoon centered at the Bay of Bengal coast and the western coast of India, the tropical western Pacific, the Pacific ITCZ , and Central America. The maximum heating exceeds 300 Wm^{-2} over the northern Bay of Bengal, and 200 Wm^{-2} over the South China Sea and the western Pacific east of the Philippines, and over Central America.

Cooling extends over much of the Southern Hemisphere (SH) subtropical latitudes and the northeastern parts of the North Pacific and Atlantic Oceans (Fig.4a). The horizontal distributions of $<Q_2>$ (Fig. 4b) and OLR flux (Fig. 4c) are similar to those of $<Q_1>$ in the tropics, indicating that the major component of heat source is latent heat released in cumulus convection. However, the differences of the values between $<Q_1>$ and $<Q_2>$ over land imply that sensible heating from

ground surface is not negligible, especially over the Asian high mountain regions including the Tibetan Plateau.

In northern fall (September - November) the major convective rainbelt and heat sources in the eastern hemisphere retreat southward and centered over the equator (Figs. 5a and 5c). They become less vigorous than in summer. Much of the Eurasian and North American continents become weak heat sinks. The southern Africa and South America become heat sources, due to the release of latent heat in deep cumulus convection as indicated by the small values of OLR ($\leq$ 240 Wm^{-2}). The Pacific ITCZ becomes wider in latitude than in summer and reaches the northmost position near 10^0N (Fig. 5c).

In summary, the large-scale features of the vertically integrated heat sources and moisture sinks obtained in this study are realistic and consistent with the OLR flux and other known features of the global circulation. The horizontal distributions and locations of the maxima/minima are generally consistent with previous estimates for corresponding seasons based on FGGE III-a analyses (Wei et al. 1983) and FGGE III-b analyses (Schaack et al. 1990) and ECMWF TOGA analyses (Schaack and Johnson 1994; Li and Yanai 1996), but with more detailed features.

4. Vertical profiles of heating

To identify the principal factors contributing to the heating or cooling more clearly, we shall examine the vertical profiles of Q_1 and Q_2 over various geographycal locations. We selected sixteen locations shown in Fig. 6 to study regional differences of heating and moistening processes.

In Figure 7, we illustrate the mean vertical profiles of Q_1 and Q_2 over land surfaces for four seasons. Over the Sahara Desert (Region A in Fig. 6) the Q_1 values show basically similar vertical distributions throughout the year, i. e., positive near the surface and negative in the upper and middle troposphere. Since little rainfall occurs in the Sahara Desert, the cooling in the middle and upper troposphere is considered to be due to radiation, while the vertical convergence of sensible heat flux explains positive values in the lower layer [see Eq. (7)]. In northern summer (June-August) Q_2 becomes positive near the surface probably due to condensation

accompanied with rains. We remark that the vertical profiles of Q_1 and Q_2 over the Australian Desert (Region P in Fig. 6) are very similar to those found over Sahara.

Figures 7D and 7E respectively show seasonal mean vertical profiles of Q_1 and Q_2 for the western and eastern Tibetan Plateau. During northern winter the Q_1 values are weakely negative indicating radiative cooling. The Q_2 values are also very small. In spring Q_1 over the Plateau becomes positive throughout the troposphere but Q_2 is negligibly small. This suggests that sensible heating from the Plateau surface is the major mechanism of heating during this season (Luo and Yanai 1984; Yanai and Li 1994a). In summer, Q_1 over the eastern Plateau shows intense heating (2 ~ 3 K day^{-1}) in the layer between 300 hPa and the surface. Q_2 is also positive (~ 1 K day^{-1}) in this layer, indicating that both sensible heating and condensation heating are contributing to the heat source as shown by Nitta (1983), Luo and Yanai (1984) and others. In fall heating over the Plateau is much reduced and Q_1 is small negative above 300 hPa, indicating radiative cooling. The profiles from northern winter to summer agree well with those of corresponding seasons obtained by Yanai et al. (1992) using the FGGE II-b data.

We also investigated the vertival profiles of Q_1 and Q_2 over the High Plains region of the western United States (Region N in Fig. 6) . During winter and spring the heating profiles are very similar to those over the western Tibetan Plateau. The radiative cooling is dominant in winter while the sensible heating becomes a major component of heat source in spring. In summer the sensible heating is still dominant over this region. In fall the radiative cooling becomes the dominant process in the upper and middle troposphere.

The vertical profiles of Q_1 and Q_2 over Brazil (Region M in Fig. 6) are distinctly different from those over dry land surface. In northern winter, spring and fall Q_1 and Q_2 values are large positive with separation of peaks in Q_1 and Q_2. As discussed by Yanai et al. (1973) and Yanai and Johnson (1993), these are the characteristics associated with rains of convective nature [see Eq. (9)]. The heating is strongest in northern winter. During northern summer, the middle and upper troposphere becomes weak heat sink and heating is confined in the lower layers.

Schaack et al. (1990) showed similar seasonal variation of the vertical distribution of heating over the central Brazil derived from the FGGE III-b analysis.

The vertical profiles of Q_1 and Q_2 over oceans (Fig. 8) also show a variety of shapes reflecting different heating and moistening processes. The vertical distributions over the Arabian Sea (Region B in Fig. 6) during northern winter, spring and fall are characterized by cooling throughout the troposphere and large negative Q_2 (moistening) in the lower layers. These are consistent with the radiative cooling discussed by Ackerman and Cox (1987) and strong evaporation from the sea surface (e.g., Rao et al. 1981; Mohanty et al. 1983). After the onset of the Indian monsoon in June, the southwest India receives rains but most of the Arabian Sea continues to experience subsidence (see Fig. 4), radiative colling and intense evaporation. Yanai et al. (1992) obtained similar profiles over the Arabian Sea using the FGGE data.

Figure 8C shows the mean vertical profiles of Q_1 and Q_2 over the region centered on the Bay of Bengal coast (Region C in Fig. 6) where the maximum heating associated with the Asian summer monsoon occurs during northern summer (see Fig. 4). In winter Q_1 is negative throughout the troposphere except near the surface. Q_2 is also negative in the troposphere. These indicate the dominance of radiative cooling and evaporation before the arrival of monsoon rains. In spring very weak heating occurs in the troposphere. During northern summer large positive values of Q_1 and Q_2 occur throughout the troposphere. The magnitudes of Q_1 and Q_2 are similar to each other, but their peaks are separated. These suggest that large heating in this region is mainly the result of latent heat released in deep cumulus clouds in the summer monsoon. The magnitude and vertical distribution of Q_1 are very similar to those obtained by Schaack et al (1990) using the FGGE III-b analysis. During fall, both Q_1 and Q_2 are substantially weakened since the major rainbelt in South Asia retreats southward to the maritime continent of Indonesia.

Figure 8H shows profiles for the region to the east of Japan over the storm tracks in the North Pacific (Region H in Fig. 6). In northern winter Q_1 is large positive in the lower tropospheric layer and decreases with height and becomes negative above 400 hPa. The behaviors of Q_2 are just opposite to those of Q_1 . Q_2 is

large negative near the surface and becomes small positive above 600 hPa. The strong low-level heating and moistening suggest strong sensible heat flux and evaporation from the warm ocean surface. In spring low-level heating and moistening are substantially weakened. During northern summer Q_1 (Q_2) becomes small negative (positive) in lower levels. In fall the vertical profiles of Q_1 and Q_2 are similar to those in winter except that their magnitudes are smaller. Similar vertical profiles of Q_1 and Q_2 and their seasonal variations are observed over the storm tracks in the North Atlantic (Region O in Fig. 6).

The profiles from the subtropical eastern South Pacific (Region K in Fig. 6) are showen in Fig. 8K. In this region the low-level anticyclonic circulation persists in all four seasons. The radiative cooling and moistening due to evaporation from the surface occur throughout the depth of the troposphere except the layer below 925hPa, where weak sensible heating appears. Schaack et al. (1990) also obtained similar vertical profiles over the subtropical eastern South Pacific using FGGE III-b analyses. Similar vertical profiles are also obtained over the subtropical eastern North Pacific and the subtropical eastern North and South Atlantic Oceans.

5. Interannual variability of heat sources

a. Relationship with ENSO

In this section we examine interannual variability of heat sources and moisture sinks. During the analysis period from 1980 to 1994, there were three major ENSO events, 1982/83, 1986/88, and 1991/92. It is well known that the ENSO events are associated with large SST anomalies and eastward or westward shift of convective activity in the tropical Pacific Ocean, and anomalous monsoon precipitation in South Asia, (e.g., Rasmusson and Carpenter 1983; Ropelewski and Halpert 1987, 1989; Krishnamurti et al. 1989, 1990).

In the following discussion the anomalies of each variable are obtained simply by subtracting the 15-year (1980-1994) mean monthly values. In order to highlight interannual variability, an 11-term low-pass filtering (Trenberth 1984) is applied to the time series of monthly anomalies of $<Q_1>$, $<Q_2>$, OLR and SST. The 11-term

filter eliminates almost completely all variations at periods less than 8 months while retaining most of the original amplitude at longer periods.

In Figures 9, 10, 11, and 12 we show the time series of low-pass filtered $<Q_1>$, $<Q_2>$, OLR and SST for four different oceanic regions. These regions are the equatorial Indian Ocean, and the western, central and eastern parts of the equatorial Pacific Ocean. For all four regions $<Q_1>$ and $<Q_2>$ curves are very close to each other, showing that release of latent heat of condensation is the primary heat source over the equatorial oceans. The amplitude of interannual variation of $<Q_1>$ increases eastward. The magnitudes of the heating and SST anomalies reach their maxima in the eastern Pacific. There is a systematic change in dominant periodicity of the $<Q_1>$ anomaly. In the equatorial Indian Ocean, short (~ 2 year) periodicity is grecognizable (Fig. 9). The short period oscillation becomes weaker in the western Pacific (Fig. 10). Over the central (Fig. 11) and eastern Pacific (Fig. 12), a longer (about 4-5 years) periodicity is evident and this low-frequency variability is remarkably well correlated with similar variations of OLR and SST. The high correlation with OLR and SST suggests that anomalous heating is the result of intensified convective activity which is favored by warmer SST.

We shall examine the horizontal distributions of the heating and OLR anomalies during the well-documented 1986/88 ENSO cycle. Figures 13 and 14 show the contrasts of the distributions of $<Q_1>$, $<Q_2>$ and OLR anomalies for the summers of 1987 and 1988. The distributions of $<Q_2>$ anomalies are very similar to those of$<Q_1>$, showing again that heating comes mainly from the release of latent heat of condensation. In the 1987 summer the warm episode reached the mature phase and large positive SST anomalies are located in the central/eastern Pacific Ocean (e.g., Kousky and Leetmaa 1989). The heating over the equatorial central Pacific is remarkably enhanced, while the heating over South Asia, Indonesia and the subtropical North Pacific is significantly weakened (Fig. 13a). Krishnamurti et al. (1989) showed that in the summer of 1987 the Indian monsoon rainfall was well below the normal. The OLR anomalies have large negative values in the central equatorial Pacific and positive values in Indonesia and the western North Pacific, indicating that deep cumulus convection has been shifted eastward to the central Pacific (Fig. 13c).

In contrast, the summer of 1988 had large negative SST anomalies (cold episode) over the equatorial central/eastern Pacific, whose magnitude and areal extent were comparable to the warm anomalies in the same region in the summer of 1987 (e.g., Kousky and Leetmaa 1989). The heating is significantly weakened over the Bay of Bengal, the South China Sea and the equatorial Pacific Ocean (Fig. 14a), where the OLR anomalies are positive indicating weaker convective activity (Fig. 14c). The heating is enhanced over the northern India, the equatorial Indian Ocean and along the SPCZ. Krishnamurti et al. (1990) showed that the Indian monsoon was stronger in the summr of 1988 and the monsoon precipitation was above the average.

b. Heating over the Tibetan Plateau

The importance of the Tibetan Plateau as an elevated heat source for the establishment and maintenance of the Asian summer monsoon circulation has been discussed by many authors [see e.g., Ye 1981; Murakami 1987; Yanai et al. 1992 for reviews]. Flohn (1957) suggested that the seasonal heating of the elevated surface of the Tibetan Plateau and the consequent reversal of the meridional temperature and pressure gradients south of the Plateau trigger the large-scale change of the general circulation over East Asia and the monsoon burst over the Indian subcontinent. Fu and Fletcher (1985) showed that the interannual variability of Indian monsoon rainfall was highly correlated with that of the thermal contrast between the Tibetan Plateau and the equatorial Pacific Ocean. Li and Yanai (1996) demonstrated that the timing and longitudinal extent of the reversal of the meridional temperature gradient south of the Tibetan Plateau vary year by year. As for the cause of the variation, Fu and Fletcher (1985) emphasized the variation of the sea surface temperature in the equatorial cold tongue. The role played by the interannual vaiations of the surface and tropospheric temperatures over the Tibetan plateau in the variation of the Asian monsoon has not been systematically studied.

In Fig. 15 we show the seasonal variation of $<Q_1>$ and $<Q_2>$ over the western Tibetan Plateau averaged over the 15 years (1980-1994), and the seasonal changes of $<Q_1>$ for individual years superimposed upon each other. Over the dry western

Plateau, the heating $<Q_1>$ does not accompany condensation process and its maximum occurs in May in agreement with the previous results (e.g., Ye and Gao 1979; Yanai et al. 1992). On the other hand, the heating over the eastern Plateau (Fig. 16) accompanies the release of latent heat of condensation during the summer months, confirming the earlier results of Nitta (1983) and Yanai and Li (1994a). For both parts of the Plateau there are substantial fluctuations of the seasonal changes in $<Q_1>$.

In Fig. 17 we show the low-pass filtered time series of $<Q_1>$ and $<Q_2>$ for both parts of the Plateau. For the western Plateau a pronounced peak of $<Q_1>$ appears during the 1990/91 winter to the 1991 summer. In both regions $<Q_1>$ and $<Q_2>$ oscillate with relatively short (1-2 years) periods. There are recognizable quasi-biennial signals in $<Q_1>$ and $<Q_2>$ over the Eastern plateau. The reason for the biennial signals is unknown at present offers an interesting question.

6. Summary and discussion

In this work we demonstrated that the simultaneous use of heat and moisture budgets applied to the recently released NCEP/NCAR reanalysis can yield a wealth of information on the global heat source distribution and its seasonal and interannual variabilities. Anlyzing the two quantities Q_1 and Q_2 (introduced in section 2) together, we gain knowledge of not only the amount of atmospheric heating but also the nature of heating (e. g., sensible heat vs. latent heat). This method was systematically utilized to interprete the results presented in sections 3 and 4. With the NCEP/NCAR reanalysis program, we can study a long term behavier of atmospheric heat sources and moisture sinks. Our work using the reanalysis (so far 1980-1994) has just started and the results on the interannual variability presented in section 5 are very preliminary.

Among many possible future research topics, we list a few on which diagnostic use of the reanalysis data may be fruitful.

In addition to the well-known ENSO-monsoon relatioship (e.g., Rasmusson and Carpenter 1983; Meehl 1987; Yasunari 1990, 1991; Webster and Yang 1992) , many

authors have found a statistical relationship between Eurasian snow cover in winter and Indian monsoon rainfall in the following summer (e.g., Hahn and Shukla 1976; Dickson 1984; Sankar-Rao et al. 1996). As Shukla (1987) noted, an inverse relationship between Eurasian snow cover and the summer monsoon is not implausible because large and persistent winter snow cover over Eurasia can delay and weaken the spring and summer heating of the land masses that is necessary for the establishment of the large-scale monsoon flow. Recently a number of numerical experiments have been carried out to test the sensitivity of the global climate system to the variability of the Eurasian snow cover (Barnett et al. 1989; Yasunari et al. 1991; Vernekar et al. 1995; Douville and Royer 1996). Their results suggest the potential importance of land processes in global climate dynamics affecting the ENSO events. Investigations of interannual variability of heating, SST and snow cover together will add a new knowledge to the understanding of ENSO/monsoon interaction.

Yanai and Li (1994b) showed that there are three distinct peaks, near 3–6 and 2–2.5 years and near 15 months in the power spectra of the monsoon intensity index (Webster and Yang 1992), the equatorial SST and the Eurasian snow cover . The quasi-biennial appearance of tropical variables such as sea level pressure (SLP), SST and precipitation has been known by many studies (e.g., Trenberth 1975; Trenberth and Shea 1987; Lau and Sheu 1988; Rasmusson et al. 1990; Jiang et al. 1996; Tomita and Yasunari 1996). The biennial tendency of the NH snow cover has been pointed out by Iwasaki (1991). Is the biennial tendency found in the heating over the Tibetan related to the biennial tendency of the snow cover? Or, is it merely a response to the biennial pulse of large-scale circulation caused by the fluctuation of SST? These are interesting questions for future reseach.

Acknowledgments. The authors thank Dr. Chengfeng Li who participated in the early phase of this research. This work was supported by the National Science Foundation under Grant ATM-9500338 and by the National Oceanic and Atmospheric Administration under Grant NA56GP0203. The computations were performed at computing facilities at NCAR/Scientific Computing Division and the Department of Atmospheric Sciences at University of California, Los Angeles.

REFERENCES

Ackerman, S. A. and S. K. Cox, 1987: Radiative energy budget estimates for the 1979 southwest summer monsoon. *J. Atmos. Sci.*, **44**, 3052-3078.

Barnett, T. P., L. Dümenil, U. Schlese, E. Roeckner, and M. Latif, 1989: The effect of Eurasian snow cover on regional and global climate variations. *J. Atmos. Sci.*, **46**, 661-685.

Christy, J. R., 1991: Diabatic heating rate estimates from European Centre for Medium-Range Weather Forecasts analyses. *J. Geophys. Res .*, **96**, 5123-5135.

Dickson, R. R., 1984: Eurasian snow cover versus Indian monsoon rainfall – An extension of the Hahn-Shukla results. *J. Climate Appl. Meteor.*, **23**, 171-173.

Dopplick, T. G., 1979: Radiative heating of the global atmosphere: Corrigendum. *J. Atmos. Sci.*, **36**, 1812-1817.

Douville, D., and J.-F. Royer, 1996: Sensitivity of the Asian summer monsoon to an anomalous Eurasian snow cover within the Meteo-France GCM. *Climate Dynamics*, **12**, 449-466.

Flohn, H., 1957: Large-scale aspects of the "summer monsoon" in South and East Asia. *J. Meteor. Soc.. Soc. Japan* (75th Ann. Vol.), 180-186.

Fu, C., and J. Fletcher, 1985: The relationship between Tibet-tropical ocean thermal contrast and interannual variability of Indian monsoon rainfall. *J. Climate Appl. Meteor.*, **24**, 841-847.

Hahn, D. G., and J. Shukla, 1976: An apparent relationship between Eurasian snow cover and Indian monsoon rainfall. *J. Atmos. Sci.*, **33**, 2461-2462.

He, H., J. W. McGinnis, Z. Song, and M. Yanai, 1987: Onset of the Asian monsoon in 1979 and the effect of the Tibetan Plateau. *Mon. Wea. Rev.*, **115**, 1966-1995.

Hoskins, B. J., H. H. Hsu, I. N. James, M. Masutani, P. D. Sardeshmukh, and G. H. White, 1989: Diagnostics of the global atmospheric circulation based on ECMWF analyses 1979-1989. World Climate Research Programme-27, WMO/TD -326, 217pp.

Iwasaki, T., 1991: Year-to-year variation of snow cover area in the Northern Hemisphere. *J. Meteor. Soc. Japan*, **69**, 209-217.

Jiang, N., J. D. Neelin, and M. Ghil, 1995: Quasi-quadrennial and quasi-biennial varability in equatorial Pacific. *Climate Dynamics*, **12**, 101-112.

Johnson, D. R., M. Yanai, and T. K. Schaack, 1987: Global and regional distributions of atmospheric heat sources and sinks during the GWE. *Monsoon Meteorology*, C. P. Chang, and T. N. Krishnamurti, Eds., Oxford University Press, 271-297.

Kalnay, E., M. Kanamitsu, R. Kistler, W. Collins, D. Deaven, L. Gandin, M. Iredell, S. Saha, G. White, J. Woollen, Y. Zhu, M. Chelliah, W. Ebisuzaki, W. Higgins, J.Janowiak, K. C. Mo, C. Ropelewski, J. Wang, A. Leetmaa, R. Reynolds, Roy Jenne, and Dennis Joseph, 1996, *Bull. Amer. Meteor. Soc.*, **77**, 437-471.

Kitoh, A., and T. Tokioka, 1987: A simulation of the tropospheric general circulation with the MRI atmospheric general circulation model. Part III: The Asian summer monsoon. *J. Meteor. Soc. Japan*, **65**, 167-187.

Kousky, V. E., and A. Leetmaa, 1989: The 1986-87 Pacific warm episode: Evolution of oceanic and atmospheric anomaly fields. *J. Climate*, **2**, 254-267.

Krishnamurti, T. N., H. S. Bedi, and M. Subramaniam, 1989: The summer monsoon of 1987. *J. Climate*, **2**, 321-340.

____, _____, _____, 1990: The summer monsoon of 1988. *Meteorol. Atmos. Phys.*, 42, 19-37.

Lau, K. M., and P. J. Sheu, 1988: Annual cycle, quasi-biennial oscillation, and Southern Oscillation. *J.Geophys. Res.*, **93**, 10,975-10,988.

Li, C., and M. Yanai, 1996: The onset and interannual variability of the Asian summer monsoon in relation to land-sea thermal contrast. *J. Climate*, **9**, 358-375.

Luo, H., and M. Yanai, 1984: The large-scale circulation and heat sources over the Tibetan Plateau and surrounding areas during the early summer of 1979. Part II: Heat and moisture budgets. *Mon. Wea. Rev.*, **112**, 966-989.

Meehl, G. A., 1987: The annual cycle and interannual variability in the tropical Pacific and Indian Ocean regions. *Mon. Wea. Rev.*, **115**, 27-50.

Mohanty, U. C., S. K. Dube and M. P. Singh, 1983: A study of heat and moisture budgets over the Arabian Sea and their role in the onset and maintenance of summer monsoons. *J. Meteor. Soc. Japan*, **61**, 208-221.

Murakami, T., 1987: Effects of the Tibetan Plateau. *Monsoon Meteorology*, C.-P. Chang and T. N. Krishnamurti, Eds., Oxford University Press, 235-270.

Nitta, T., 1977: Response of cumulus updraft and downdraft to GATE A/B-scale motion systems. *J. Atmos. Sci.*, **34**, 1163-1186.

_____, 1983: Observational study of heat sources over the eastern Tibetan Plateau during the summer monsoon. *J. Meteor. Soc. Japan*, **61**, 590-605.

Rao, G. V., W. R. Schaub, Jr., and J. Puetz, 1981: Evaporation and precipitation over the Arabian Sea during several monsoon seasons. *Mon. Wea. Rev.*, **109**, 364-370.

Rasmusson, E. M., and T. H. Carpenter, 1983: The relationship between the eastern equatorial Pacific sea surface temperatures and rainfall over India and Sri Lanka. *Mon. Wea. Rev.*, **111**, 517-528.

_____, X. Wang, and C. F. Ropelewski, 1990: The biennial component of ENSO variability. *J. Marine System*, **1**, 71-96.

Ropelewski, C. F., 1988: The global climate for June-August 1988: A swing to the positive phase of the Southern Oscillation, drought in the United States, and abundant rain in monsoon areas. *J. Climate*, **1**, 1153-1174.

_____, and M. S. Halpert, 1987: Global- and regional-scale precipitation patterns associated with the El Nino/Southern Oscillation. *Mon. Wea. Rev.*, **115**, 1606-1626.

_____, and _____, 1989: Precipitation patterns associated with the high index phase of the Southern Oscillation. *J. Climate*, **2**, 268-284.

Sankar-Rao, M., K. M. Lau, and S. Yang, 1996: On the relationship between Eurasian snow cover and the Asian monsoon. *International J. Climatology*, (in press).

Schaack, T. K., and D. R. Johnson, 1994: January and July global distributions of atmospheric heating for 1986, 1987, and 1988. *J. Climate*, **7**, 1270-1285.

_____, and _____, and M.-Y. Wei, 1990: The three-dimensional distribution of atmospheric heating during the GWE. *Tellus*, **42A**, 305-327.

Shukla, J., 1987: Interannual variability of monsoons. *Monsoons*, J. S. Fein and P. L. Stephens, Eds., John Wiley & Sons, 399-463.

Tomita, T., and T. Yasunari, 1996: Role of the northeast winter monsoon on the biennial oscillation of the ENSO/monsoon system. *J. Meteor. Soc. Japan*, **74**, (in press).

Trenberth, K. E., 1975: A quasi-biennial standing wave in the Southern Hemisphere and interrelations with sea surface temperature. *Quart. J. Roy. Meteor. Soc.*, **101**, 55-74.

_____, 1984: Signal versus noise in the southern oscillation. *Mon. Wea. Rev.*, **112**, 326-332.

_____, 1992: Global analyses from ECMWF and atlas of 1000 to 10 mb circulation statistics. NCAR Tech. Note, NCAR/TN-373+STR, 191 pp.

_____, and J. G. Olson, 1988: ECMWF global analyses 1976-86: Circulation statistics and data evalution. NCAR Tech. Note, NCAR/TN-300+STR, 94 pp. plus 12 fiche.

_____, and D. J. Shea, 1987: On the evolution of the southern Oscillation. *Mon. Wea. Rev.*, **115**, 3078-3096.

_____, and A. Solomon, 1994: The global heat balance: heat transports in the atmosphere and ocea. *Climate Dynamics*, **10**, 107-134.

Vernekar, A. D., J. Zhou, and J. Shukla, 1995: The effect of Eurasian snow cover on the Indian monsoon. *J. Climate*, **8**, 248-266.

Webster, P. J., and S. Yang, 1992: Monsoon and ENSO: Selectively interactive systems. *Quart. J. Roy. Meteor. Soc.*, **118**, 877-926.

Wei, M.-Y., D. R. Johnson, and R. D. Townsend, 1983: Seasonal distributions of diabatic heating during the First GARP Global Experiment. *Tellus*, **35A**, 241-255.

Yanai, M., and R. H. Johnson, 1993: Impacts of cumulus convection on thermodynamic fields. *The Representation of Cumulus Convection in Numerical Models of the Atmosphere*, K. A. Emanuel and D. J. Raymond, Eds., American Meteorological Society, 39-62.

_____, and C. Li, 1994a: Mechanism of heating and the boundary layer over the Tibetan Plateau. *Mon. Wea. Rev.*, **122**, 305-323.

_____, and _____, 1994b: Interannual variability of the Asian summer monsoon and its relationship with ENSO, Eurasian snow cover and heating. Proc. International Conference on Monsoon Variability and Prediction. Trieste, Italy, 9-13 May 1994. WMO/TD No. 619, Vol. I, 27-34.

_____, and ____, 1996: Seasonal and interannual variability of athmospheric heating. Preprint Volume of the Eighth Conference on Air-Sea Interaction and Symposium on GOALS, 28 January - 2 February 1996, Atlanta, GA, American Meteorological Society, 102-106.

_____, S. Esbensen and J.-H. Chu, 1973: Determination of bulk properties of tropical cloud clusters from large-scale heat and moisture budgets. *J. Atmos. Sci.*, **30**, 611-627.

_____, C. Li, and Z. Song, 1992: Seasonal heating of the Tibetan Plateau and its effects on the evolution of the Asian summer monsoon. *J. Meteor. Soc. Japan,* **70,** 319-351.

Yang, S., 1996: ENSO-snow-monsoon associations and seasonal-interannual predictions. *International J. Climatology,* **16,** 125-134.

Yasunari, T., 1990: Impact of Indian monsoon on the coupled atmosphere/ocean system in the tropical Pacific. *Meteor. Atmos. Phys.,* **44,** 29-41.

_____, 1991: The monsoon year – A new concept of the climatic year in the tropics. *Bull. Amer. Meteor. Soc.,* **72,** 1331-1338.

_____, A. Kitoh, and T. Tokioka, 1991: Local and remote responses to excessive snow mass over Eurasia appearing in the northern spring and summer climate – A study with the MRI-GCM –. *J. Meteor. Soc. Japan,* **69,** 473-487.

Ye, D. (Yeh, T.-C.), 1981: Some characteristics of the summer circulation over the Qinghai-Xizang (Tibet) Plateau and its neighborhood. *Bull. Amer. Meteor. Soc.,* **62,** 14-19.

_____, and Y. X. Gao, 1979: *The Meteorology of the Qinghai-Xizang (Tibet) Plateau.* Science Press, Beijing, 278 pp. [in Chinese].

Figure legends

Fig. 1. Time series of the monthly mean values of (a) vertically integrated heat source $<Q_1>$ (solid line) and moisture sink $<Q_2>$ (dashed line), and (b) zonal wind component at 850 hPa (solid) and 200 hPa (dashed), averaged over the area 85^0E-105^0E, 5^0N-25^0N.

Fig. 2. Global distributions of the 15-year mean (1980-94) (a) vertically integrated heat source $<Q_1>$, (b) vertically integrated moisture sink $<Q_2>$ and (c) OLR flux (units: W m^{-2}) for northern winter (December, January, February) .

Fig. 3. As in Fig. 2 but for northern spring (March, April, May).

Fig. 4. As in Fig. 2 but for northern summer (June, July, August).

Fig. 5. As in Fig. 2 but for northern fall (September, October, November).

Fig. 6. Geographical locations where the vertical profiles of heat source Q_1 and moisture sink Q_2 are examined.

Fig. 7. Seasonal mean vertical profiles of heat source Q_1 and moisture sink Q_2 averaged for various regions over land. (A) Sahara, (D) western Tibetan Plateau, (E) eastern Tibetan Plateau, and (M) Brazil.

Fig. 8. As in Fig. 7 but for various regions over oceans. (B) the Arabian Sea, (C) the Bay of Bengal, (H) off east coast of Japan, and (K) subtropical eastern South Pacific.

Fig. 9. Time series of the monthly mean anomalies of (a) $<Q_1>$ (solid) and $<Q_2>$ (dashed), (b) OLR, and (c) SST for the equatorial Indian Ocean. (Units: W m^{-2} for $<Q_1>$, $<Q_2>$ and OLR, ^{0}C for SST).

Fig. 10. As in Fig. 9 but for the equatorial western Pacific.

Fig. 11. As in Fig. 9 but for the equatorial central Pacific.

Fig. 12. As in Fig. 9 but for the equatorial eastern Pacific.

Fig. 13. Distributions of the anomalies of (a) $<Q_1>$, (b) OLR flux and (c) SST for the summer of 1987. (Units: W m^{-2} for $<Q_1>$ and OLR, ^{0}C for SST).

Fig. 14. As in Fig. 13 but for the summer of 1988.

Fig. 15. (a) The 15 year (1980-1994) mean seasonal changes of $<Q_1>$ and $<Q_2>$ and (b) interannual variation of the seasonal change in $<Q_1>$ over the western Tibetan Plateau.

Fig. 16. As in Fig. 15 but for the eastern Tibetan Plateau.

Fig. 17. Time series of monthly mean anomalies of $<Q_1>$ and $<Q_2>$ over (a) the western Tibetan Plateau, and (b) the eastern Tibetan Plateau.

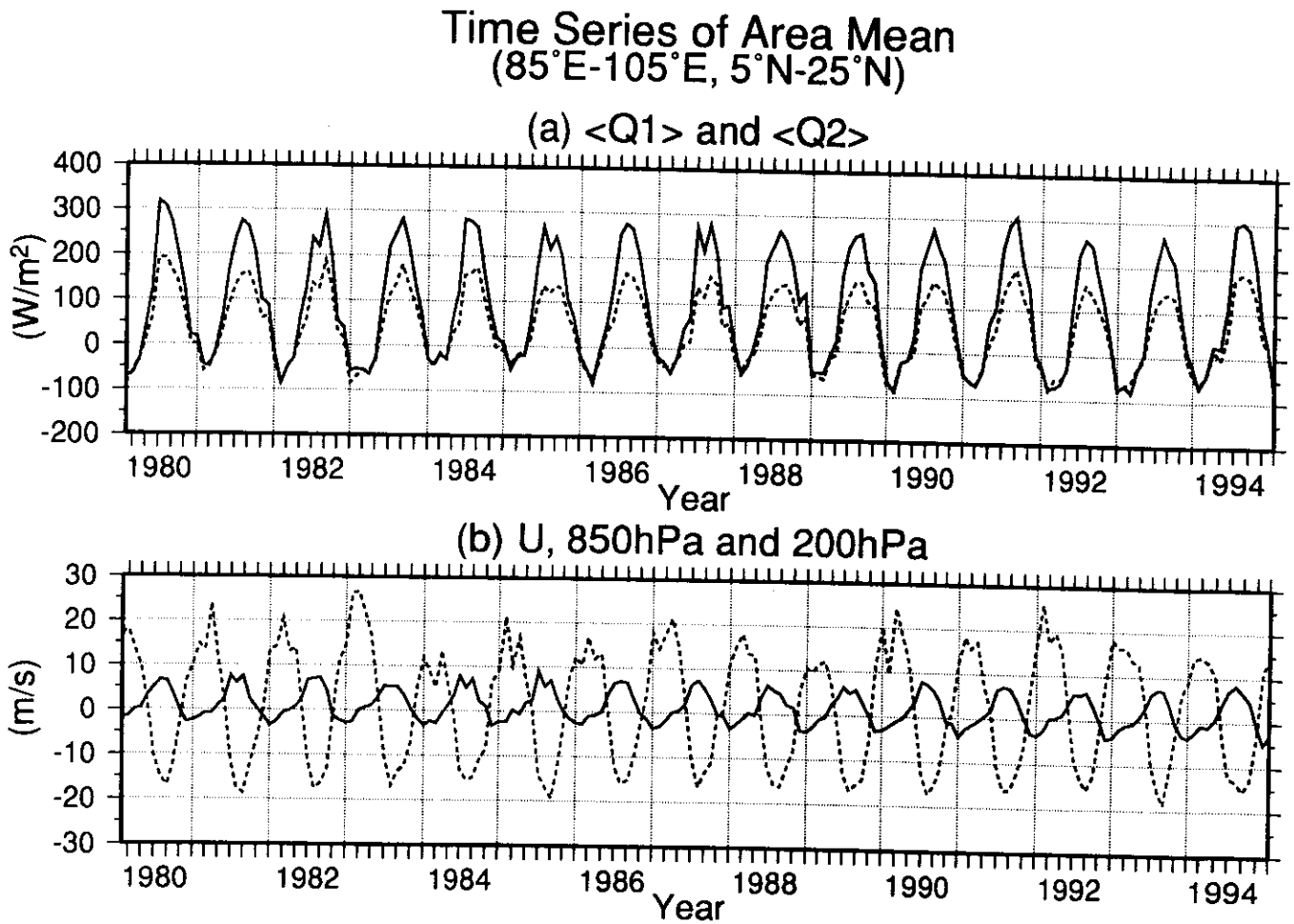

Fig. 1. Time series of the monthly mean values of (a) vertically integrated heat source $<Q_1>$ (solid line) and moisture sink $<Q_2>$ (dashed line), and (b) zonal wind component at 850 hPa (solid) and 200 hPa (dashed), averaged over the area 85^0E-105^0E, 5^0N-25^0N.

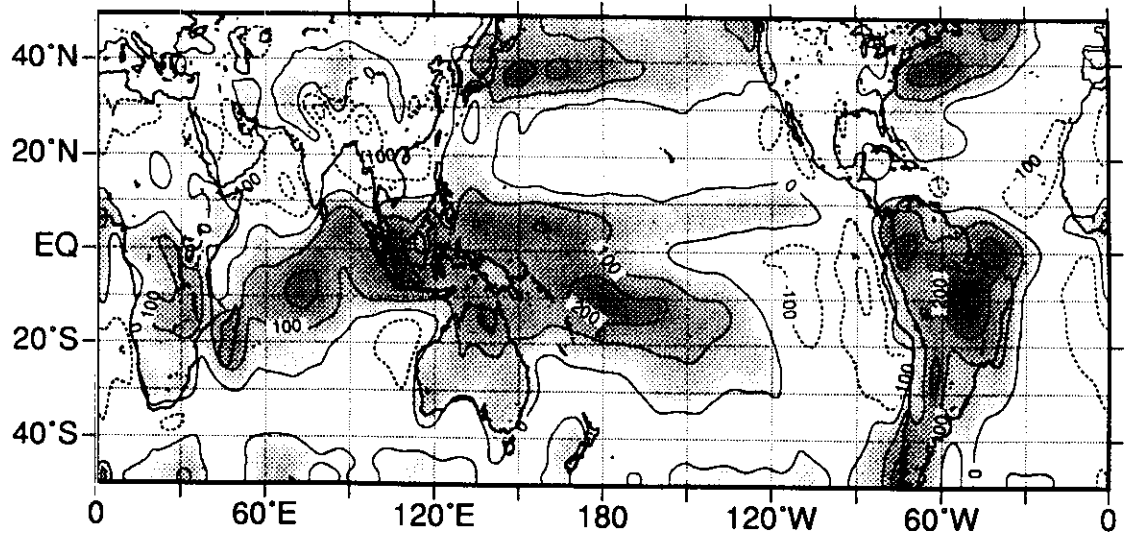

(b) <Q2> 1980-94 Winter

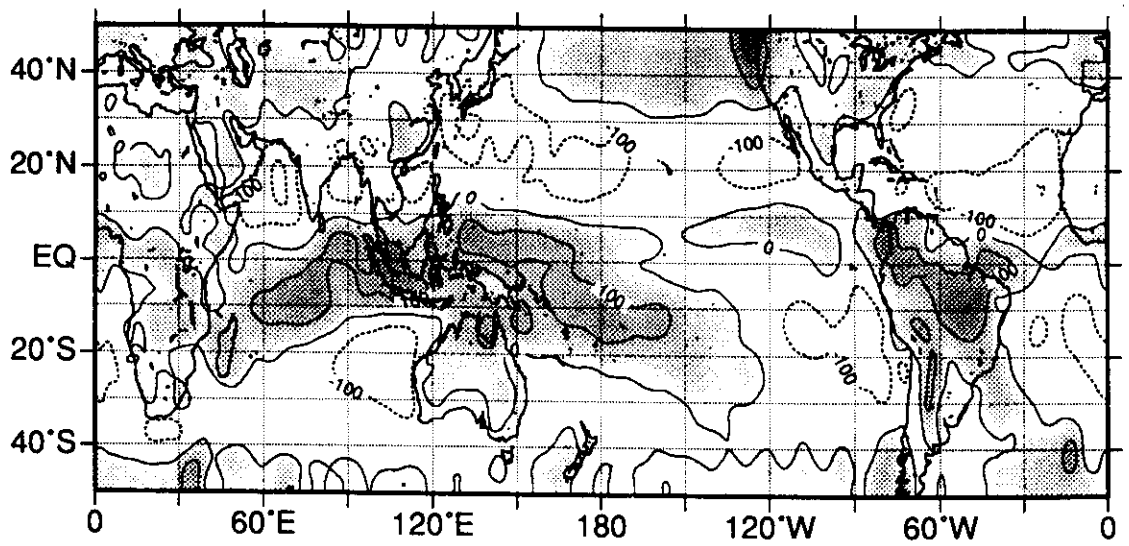

(c) OLR 1980-94 Winter

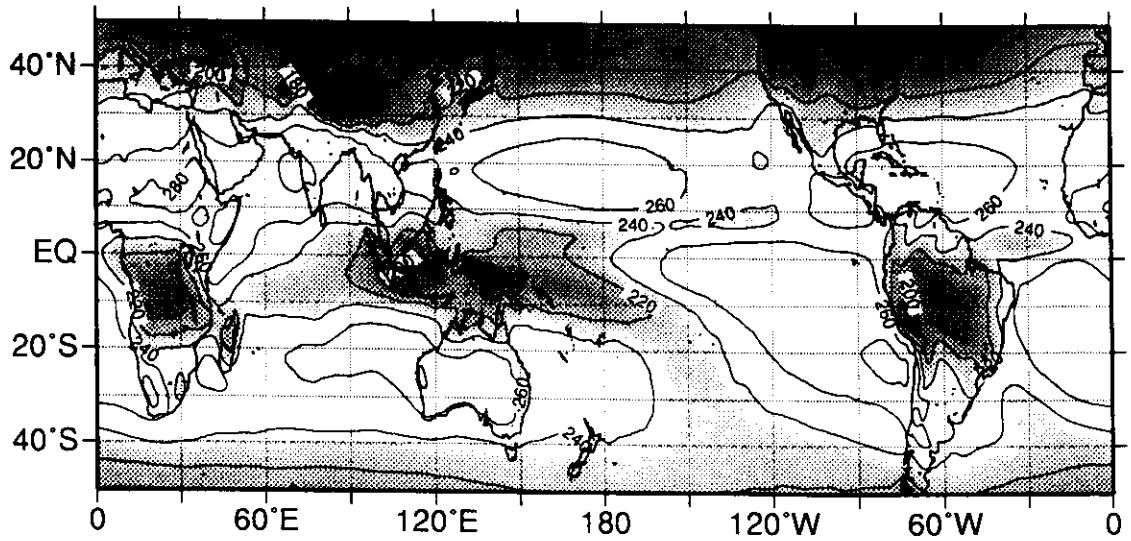

Fig. 2. Global distributions of the 15-year mean (1980-94) (a) vertically integrated heat source $<Q_1>$, (b) vertically integrated moisture sink $<Q_2>$ and (c) OLR flux (units: W m^{-2}) for northern winter (December, January, February) .

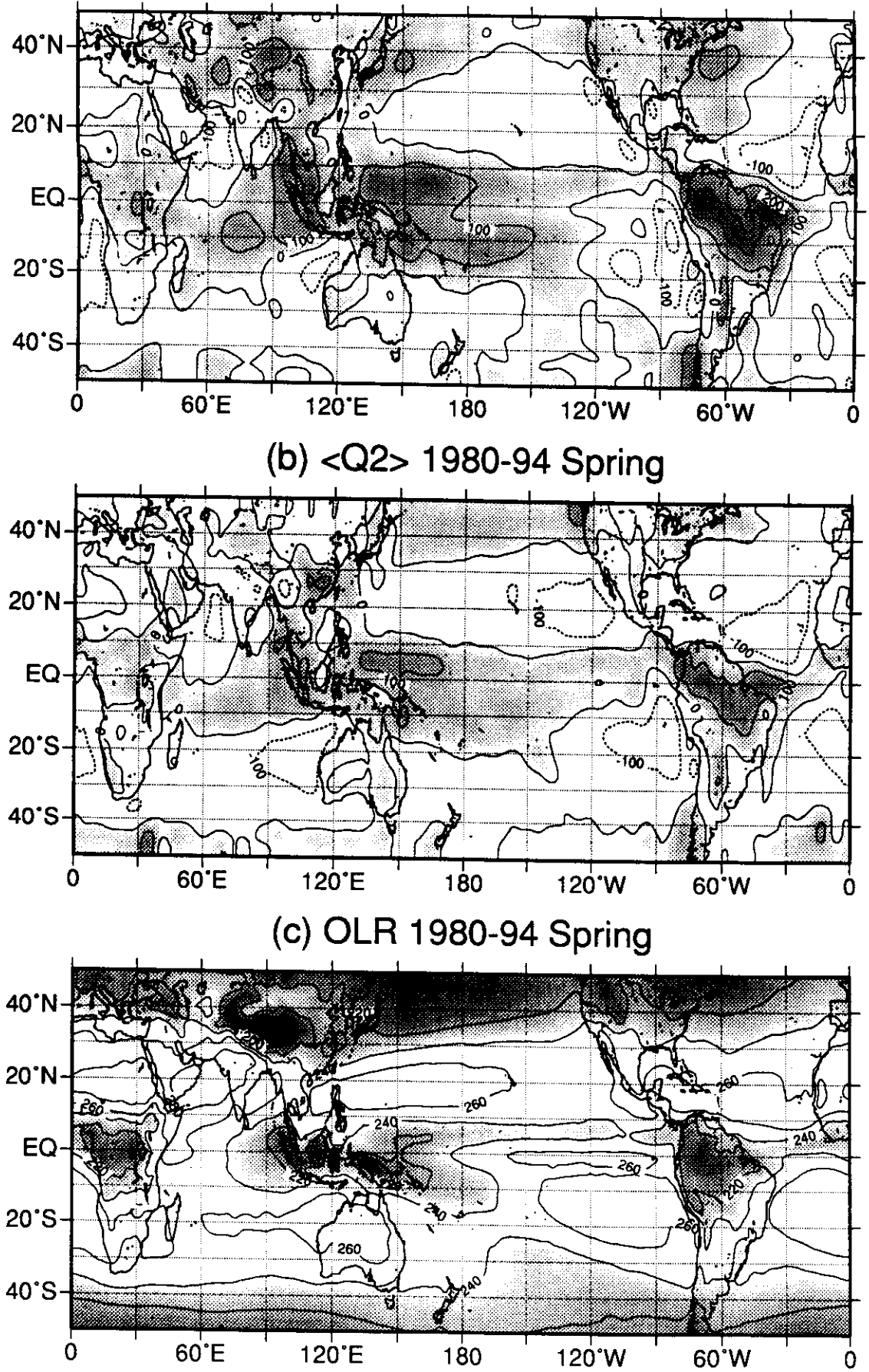

Fig. 3. As in Fig. 2 but for northern spring (March, April, May).

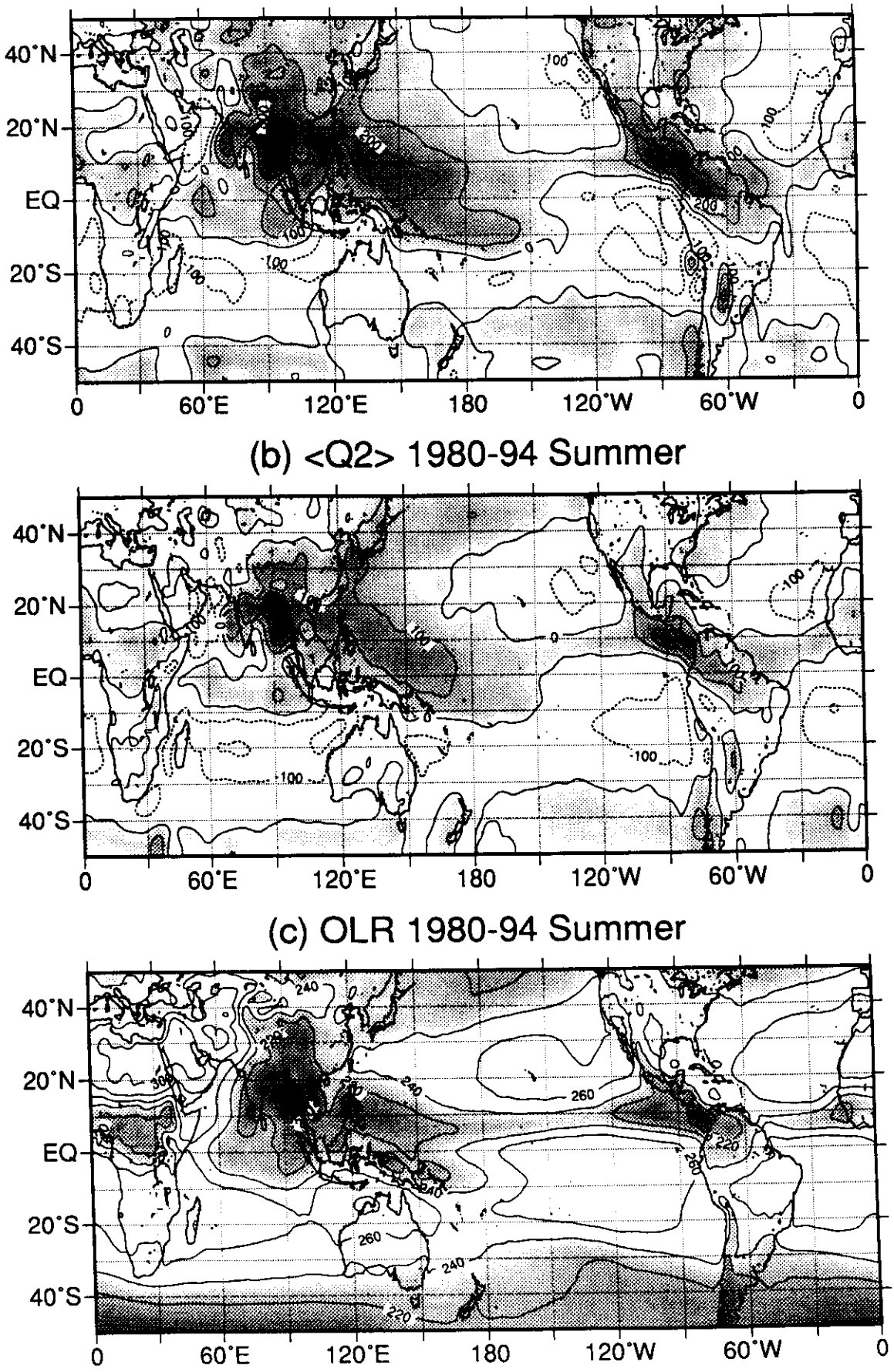

Fig. 4. As in Fig. 2 but for northern summer (June, July, August).

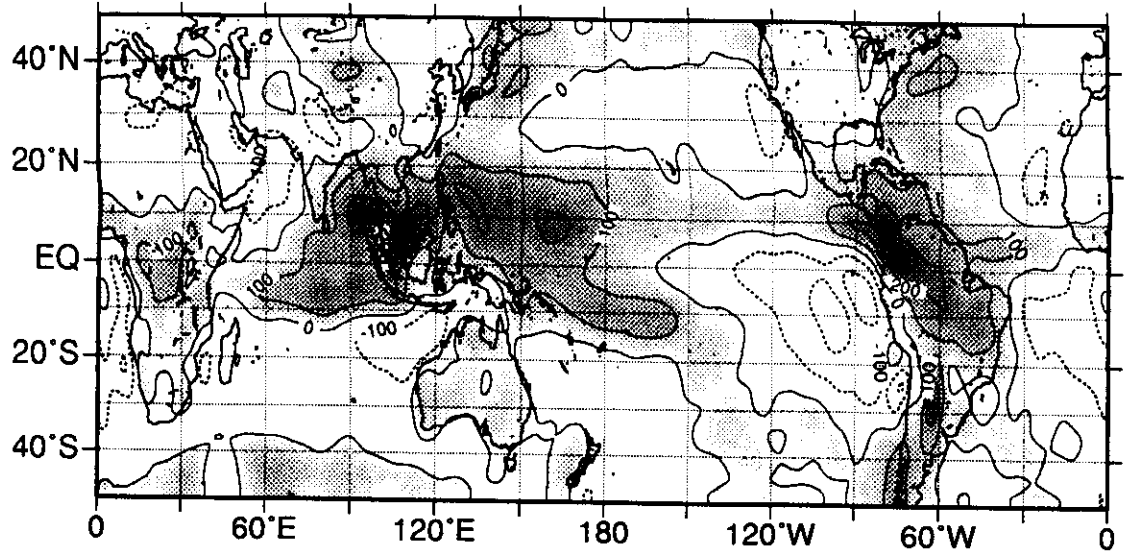

(b) <Q2> 1980-94 Autumn

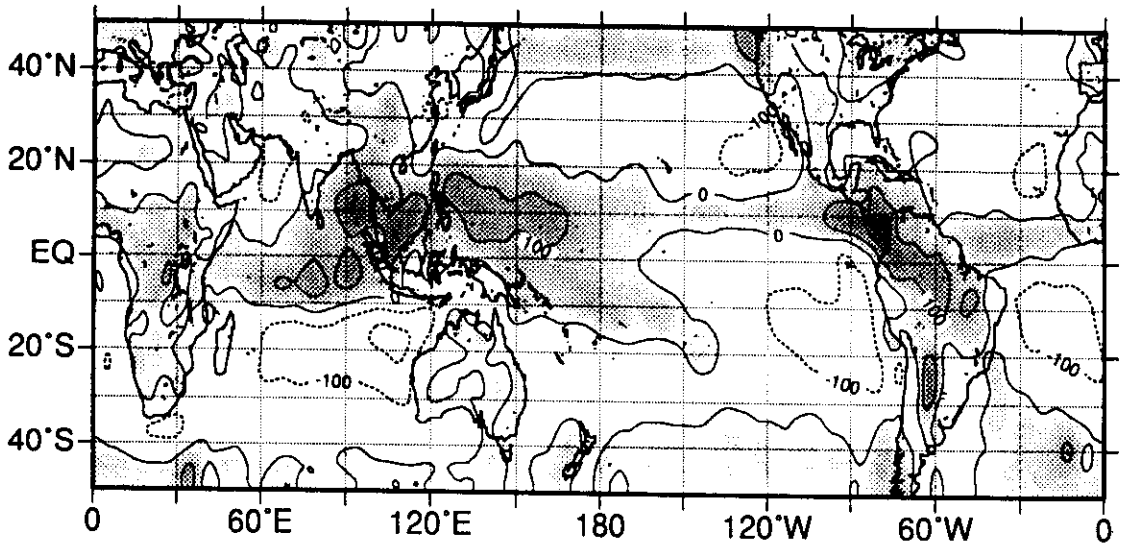

(c) OLR 1980-94 Autumn

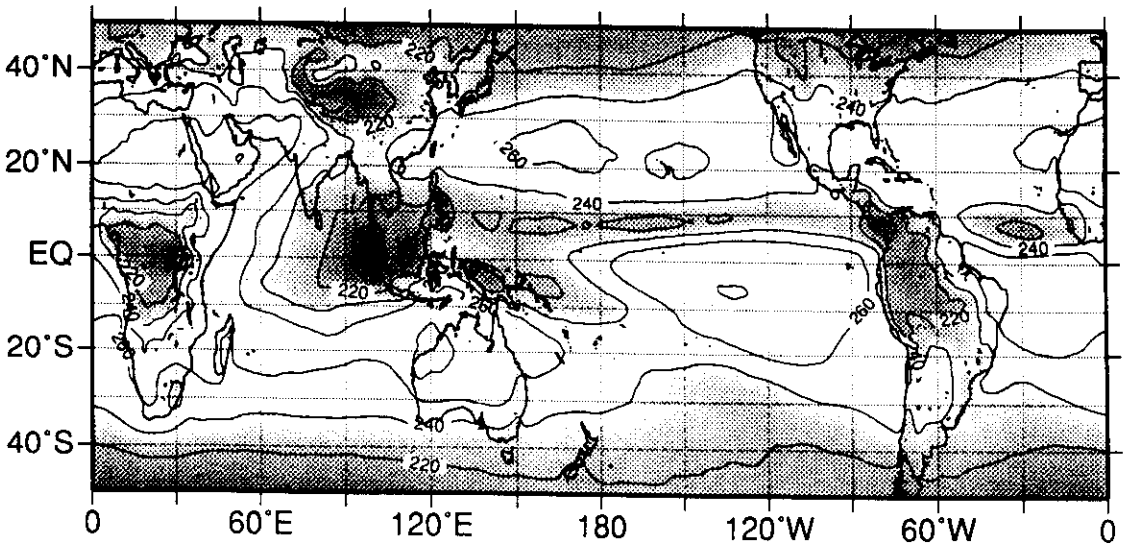

Fig. 5. As in Fig. 2 but for northern fall (September, October, November).

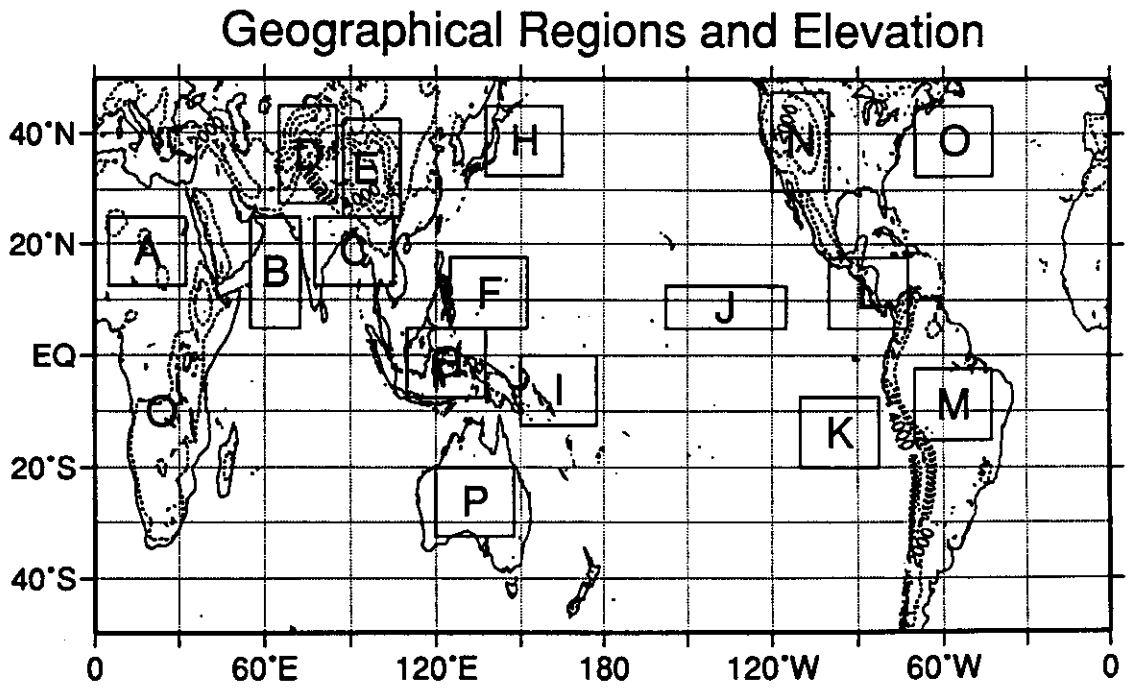

Fig. 6. Geographical locations where the vertical profiles of heat source Q_1 and moisture sink Q_2 are examined.

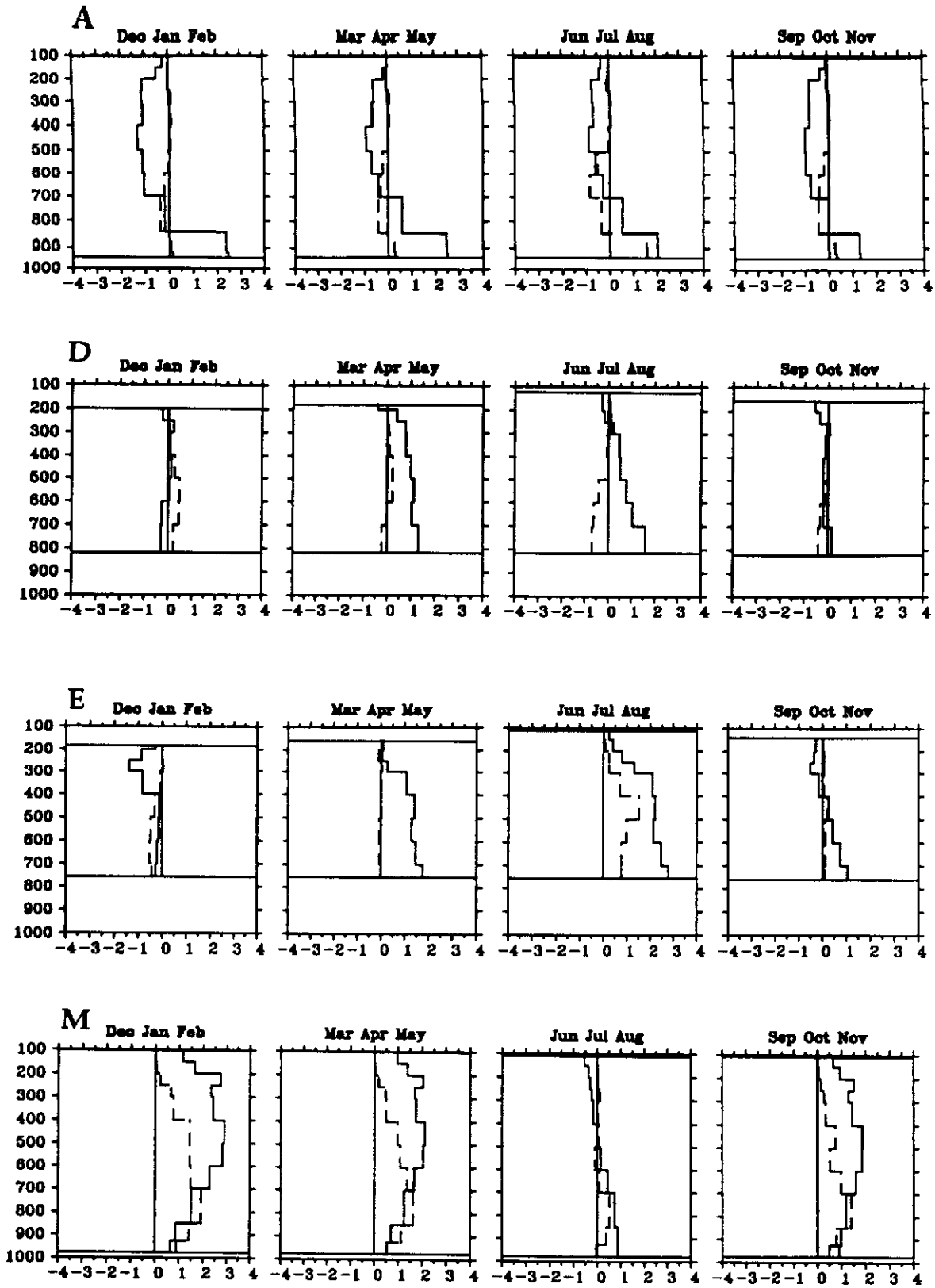

Fig. 7. Seasonal mean vertical profiles of heat source Q_1 and moisture sink Q_2 averaged for various regions over land. (A) Sahara, (D) western Tibetan Plateau, (E) eastern Tibetan Plateau, and (M) Brazil.

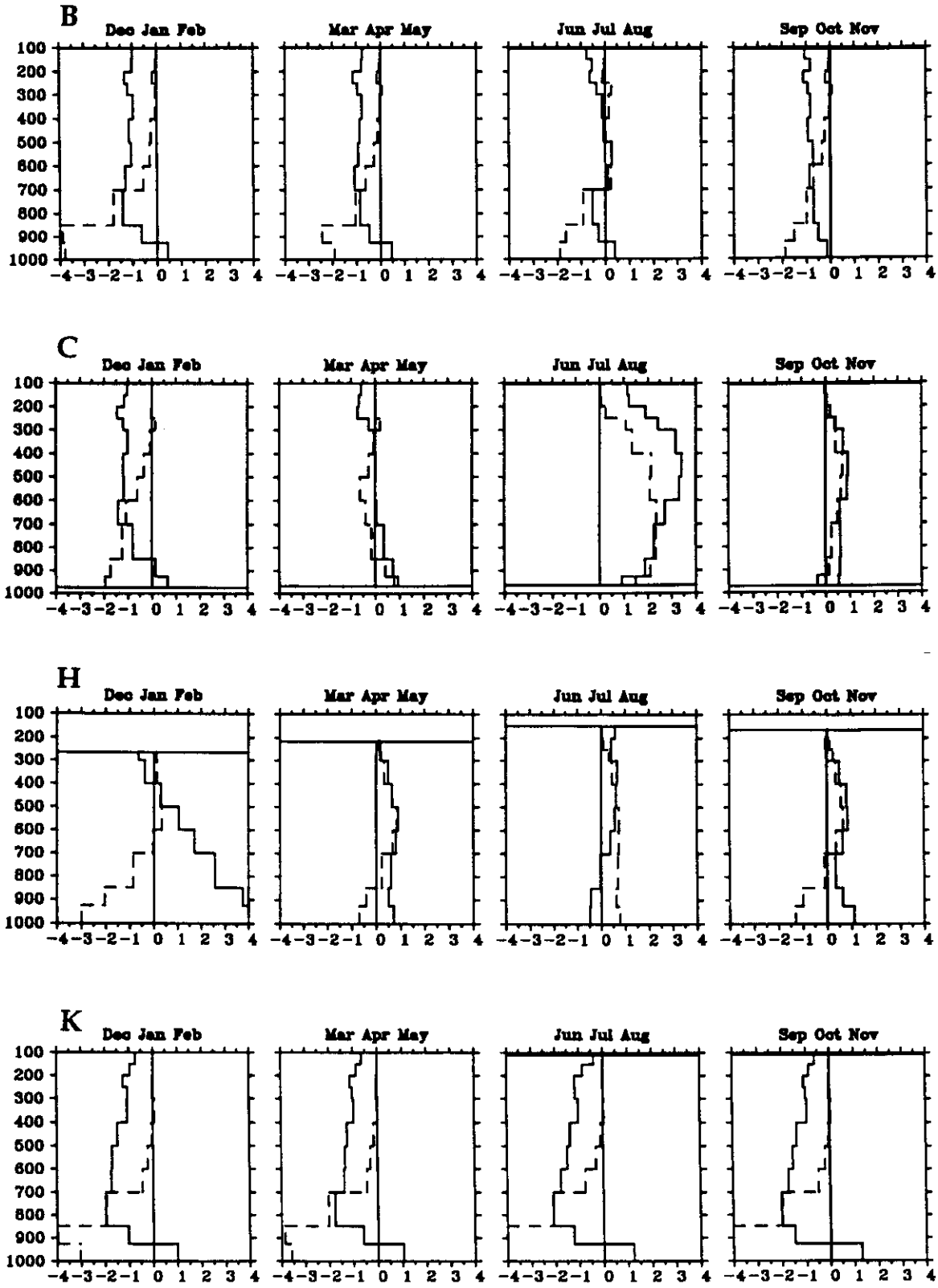

Fig. 8. As in Fig. 7 but for various regions over oceans. (B) the Arabian Sea, (C) the Bay of Bengal, (H) off east coast of Japan, and (K) subtropical eastern South Pacific.

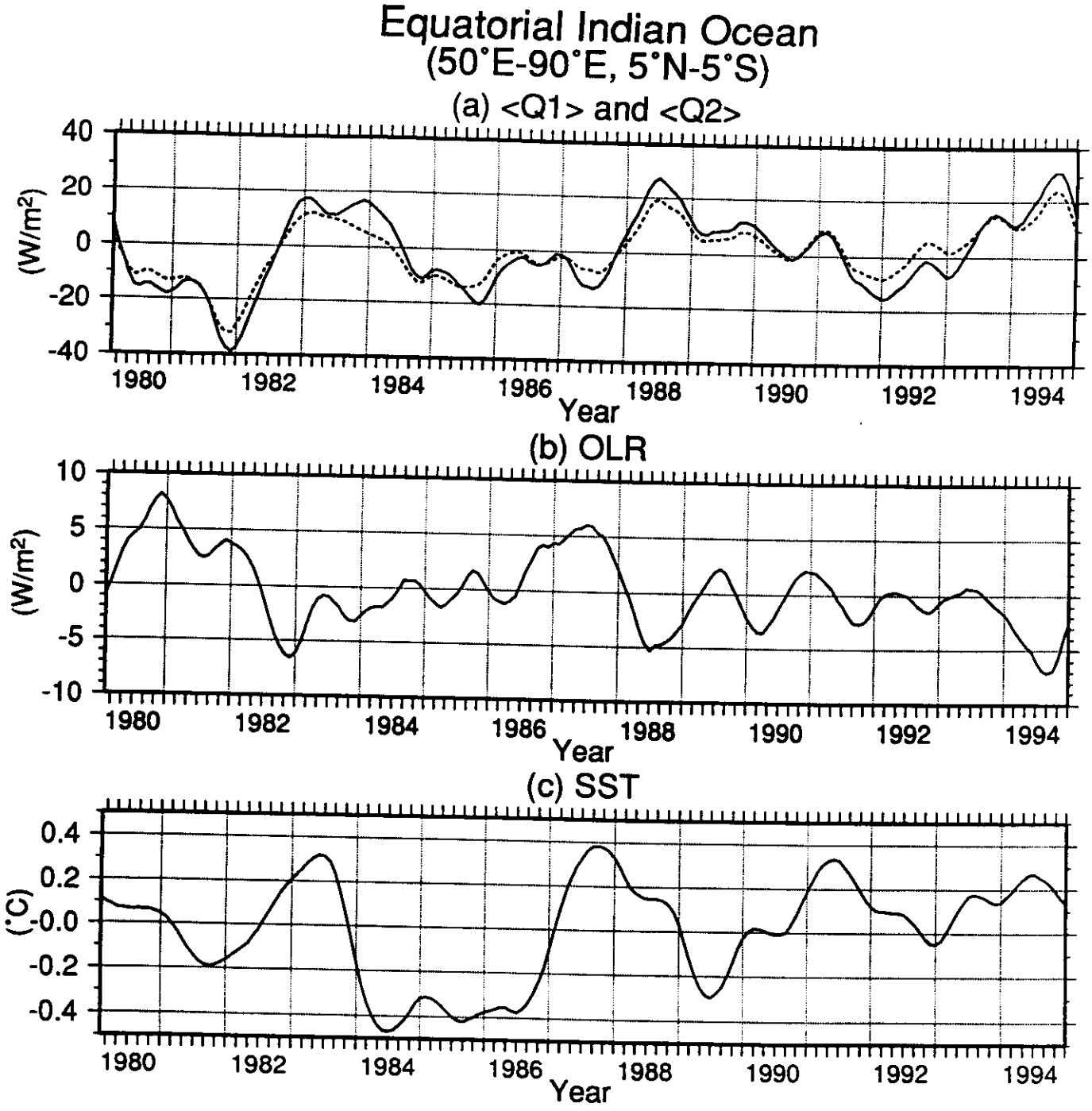

Fig. 9. Time series of the monthly mean anomalies of (a) $<Q_1>$ (solid) and $<Q_2>$ (dashed), (b) OLR, and (c) SST for the equatorial Indian Ocean. (Units: W m^{-2} for $<Q_1>$, $<Q_2>$ and OLR, ^{0}C for SST).

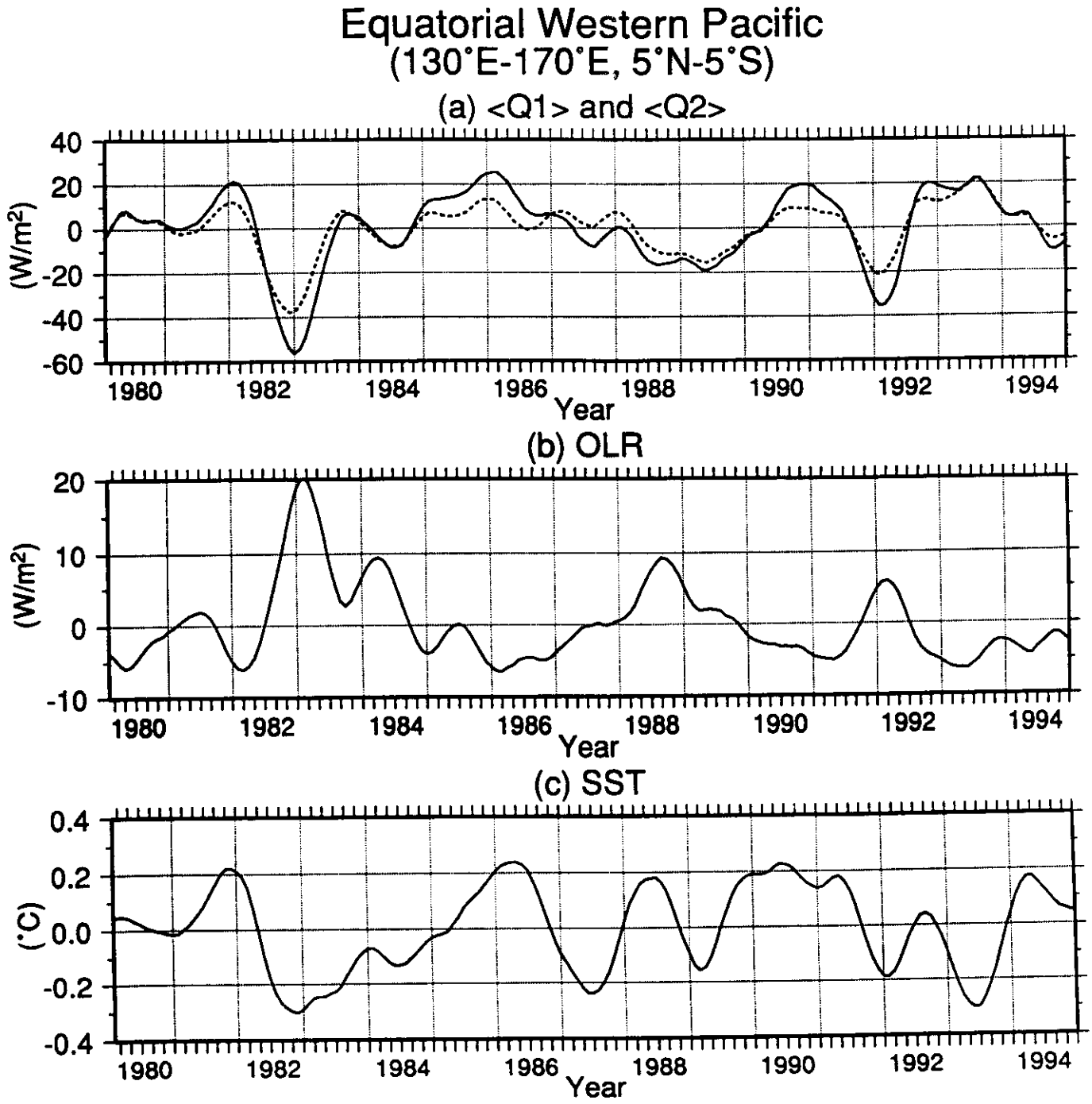

Fig. 10. As in Fig. 9 but for the equatorial western Pacific.

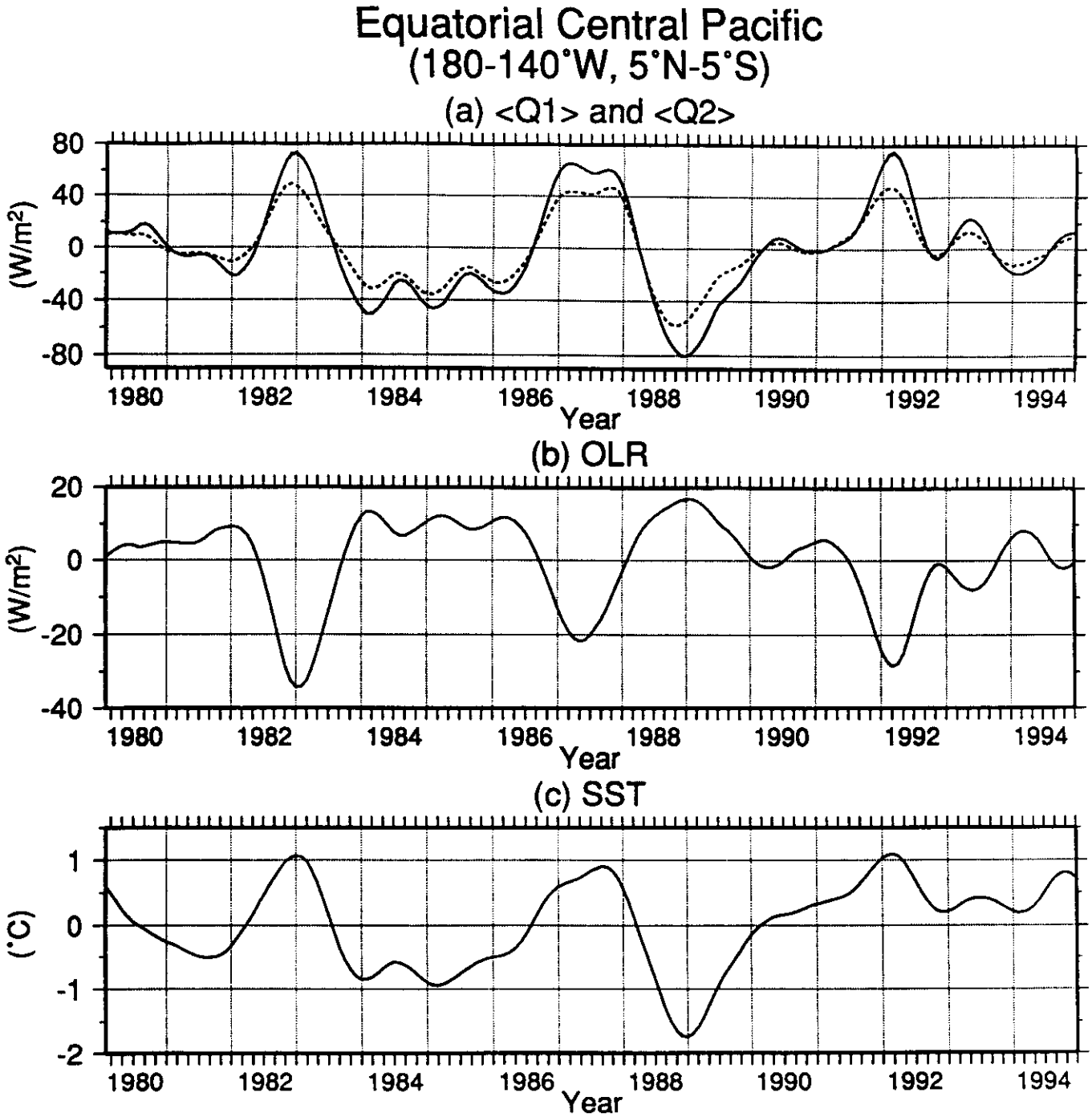

Fig. 11. As in Fig. 9 but for the equatorial central Pacific.

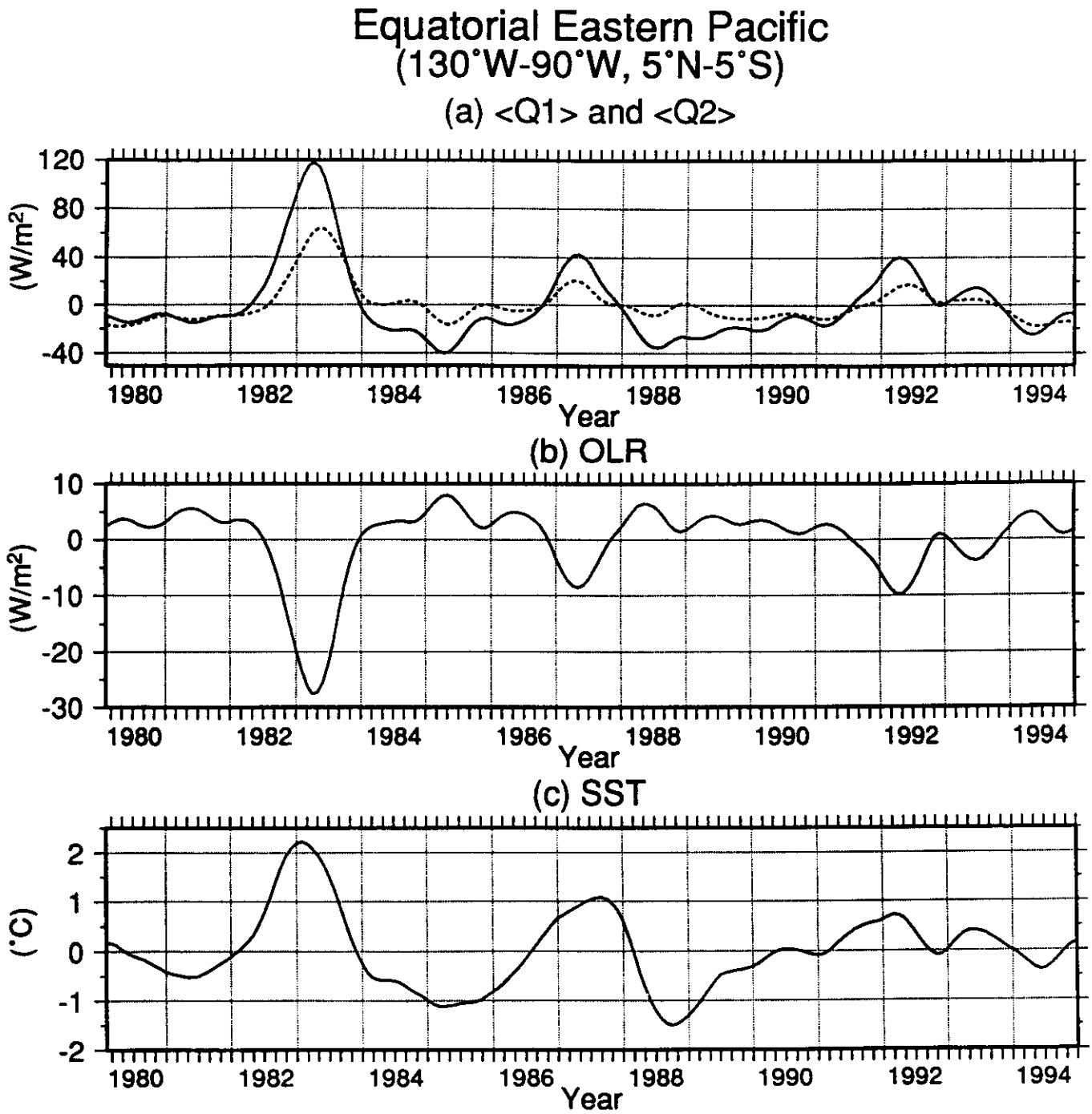

Fig. 12. As in Fig. 9 but for the equatorial eastern Pacific.

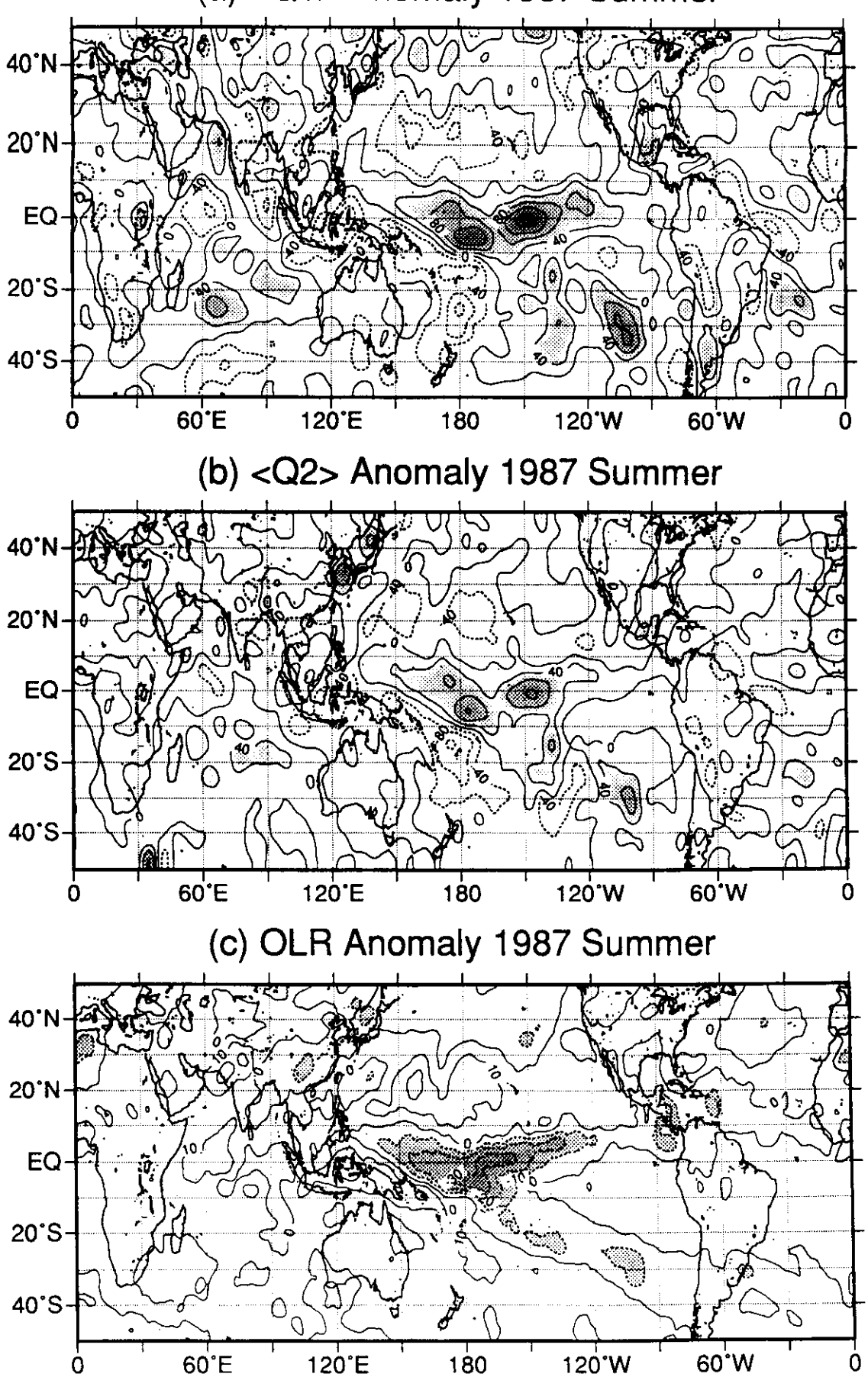

Fig. 13. Distributions of the anomalies of (a) $<Q_1>$, (b) OLR flux and (c) SST for the summer of 1987. (Units: W m^{-2} for $<Q_1>$ and OLR , ^{0}C for SST).

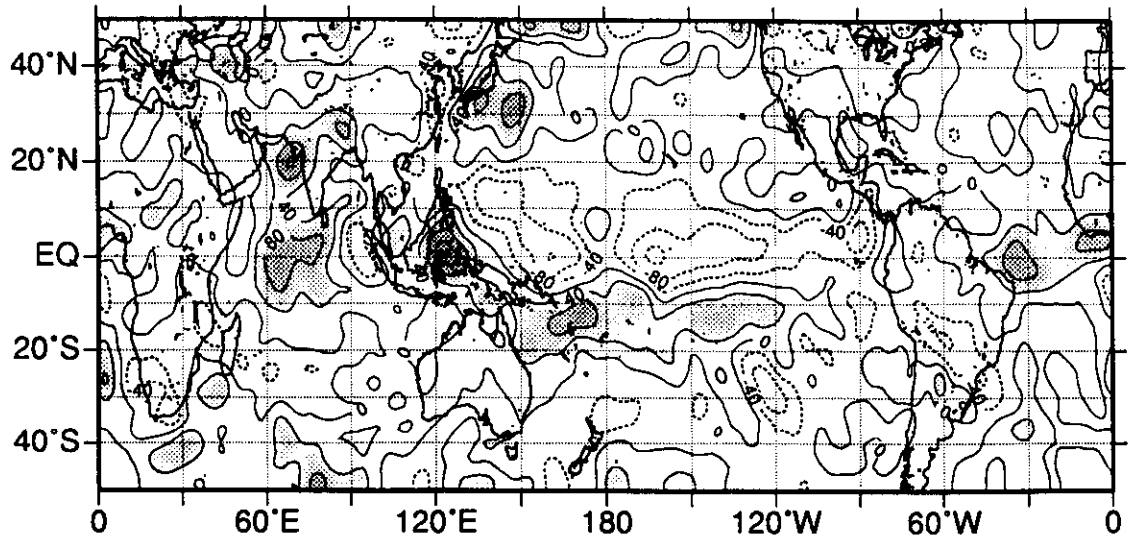

(b) <Q2> Anomaly 1988 Summer

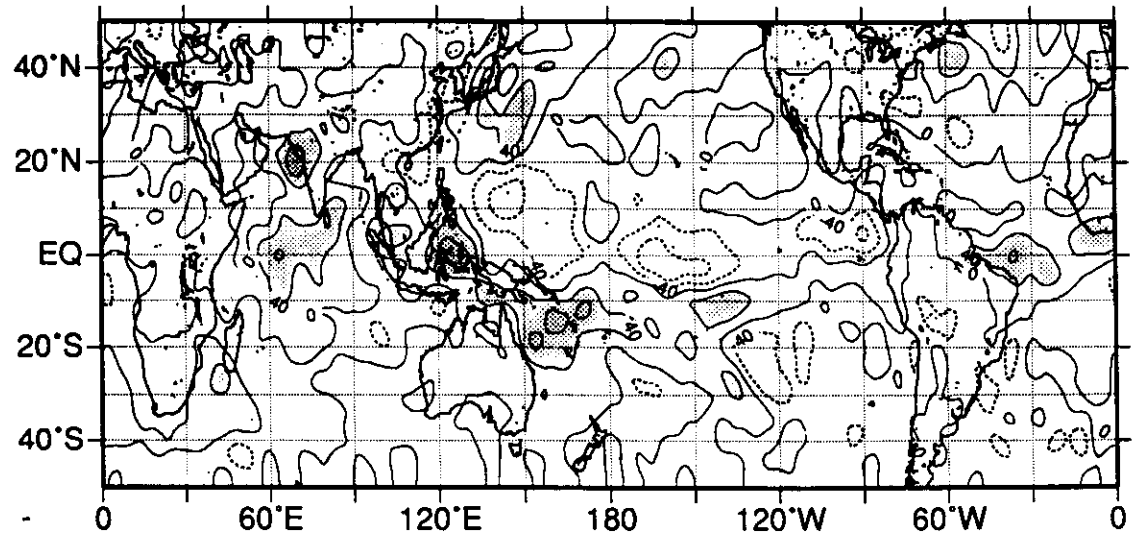

(c) OLR Anomaly 1988 Summer

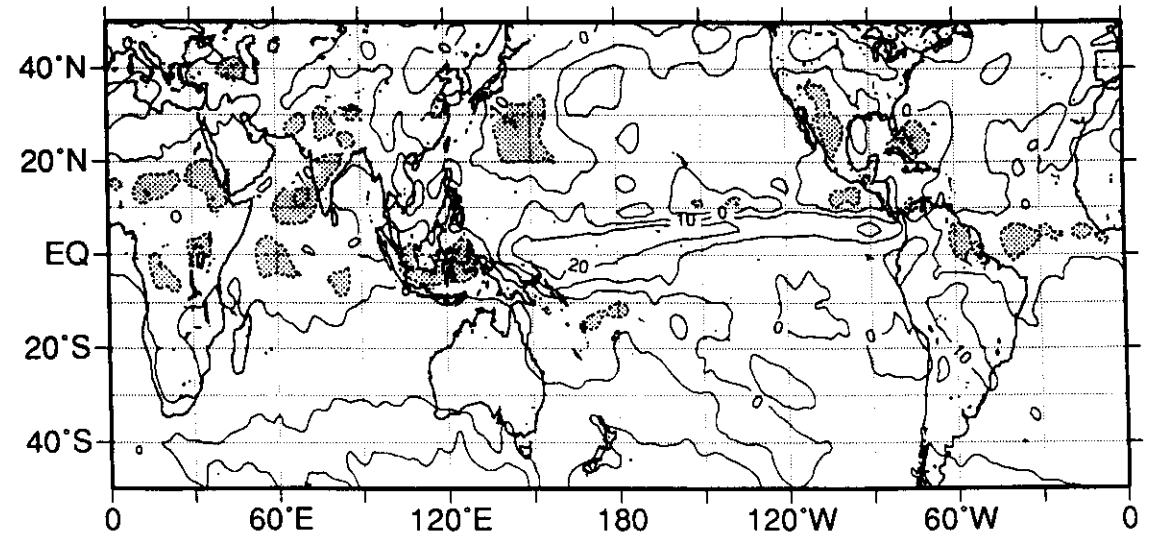

Fig. 14. As in Fig. 13 but for the summer of 1988.

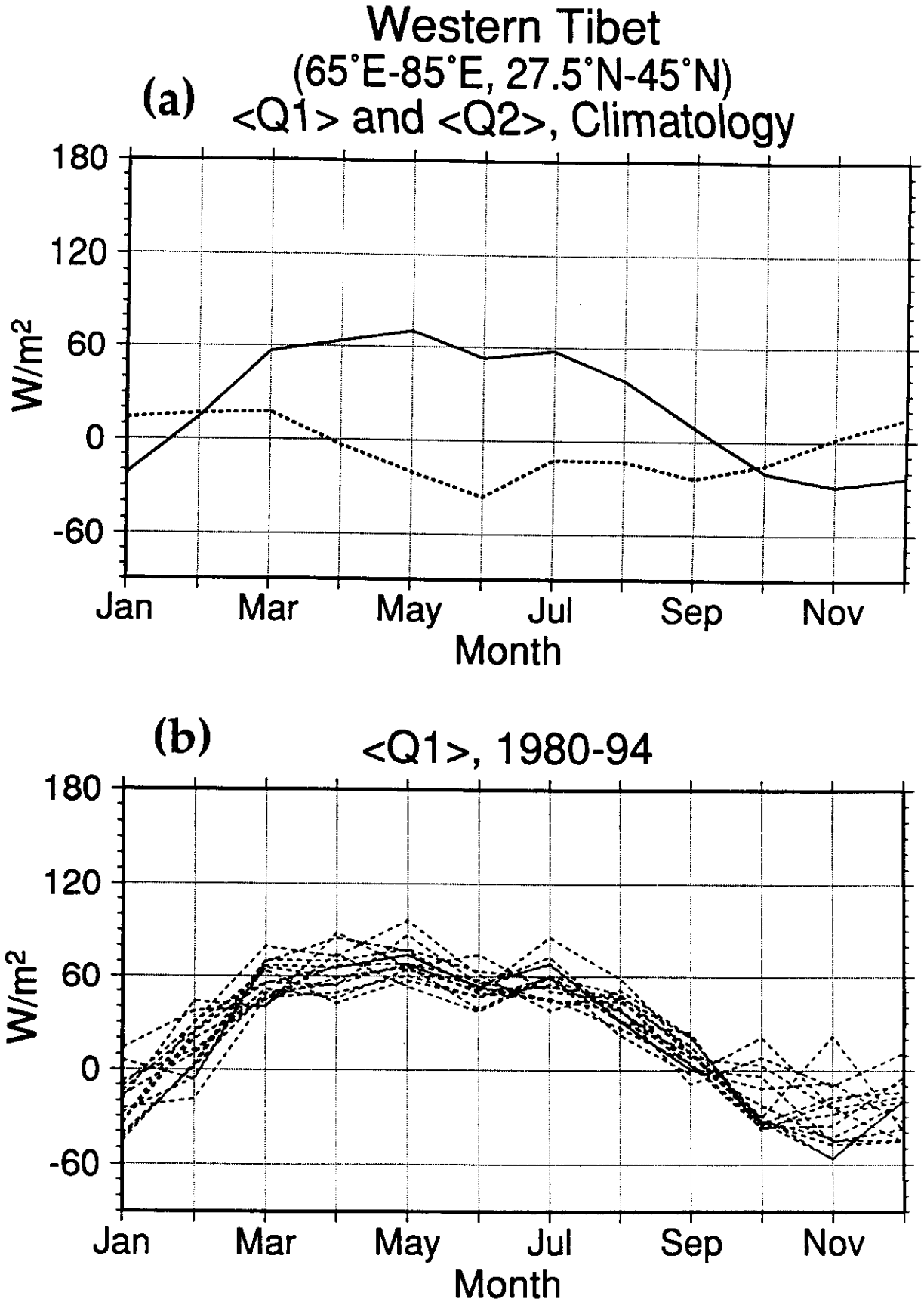

Fig. 15. (a) The 15 year (1980-1994) mean seasonal changes of $<Q_1>$ and $<Q_2>$ and (b) interannual variation of the seasonal change in $<Q_1>$ over the western Tibetan Plateau.

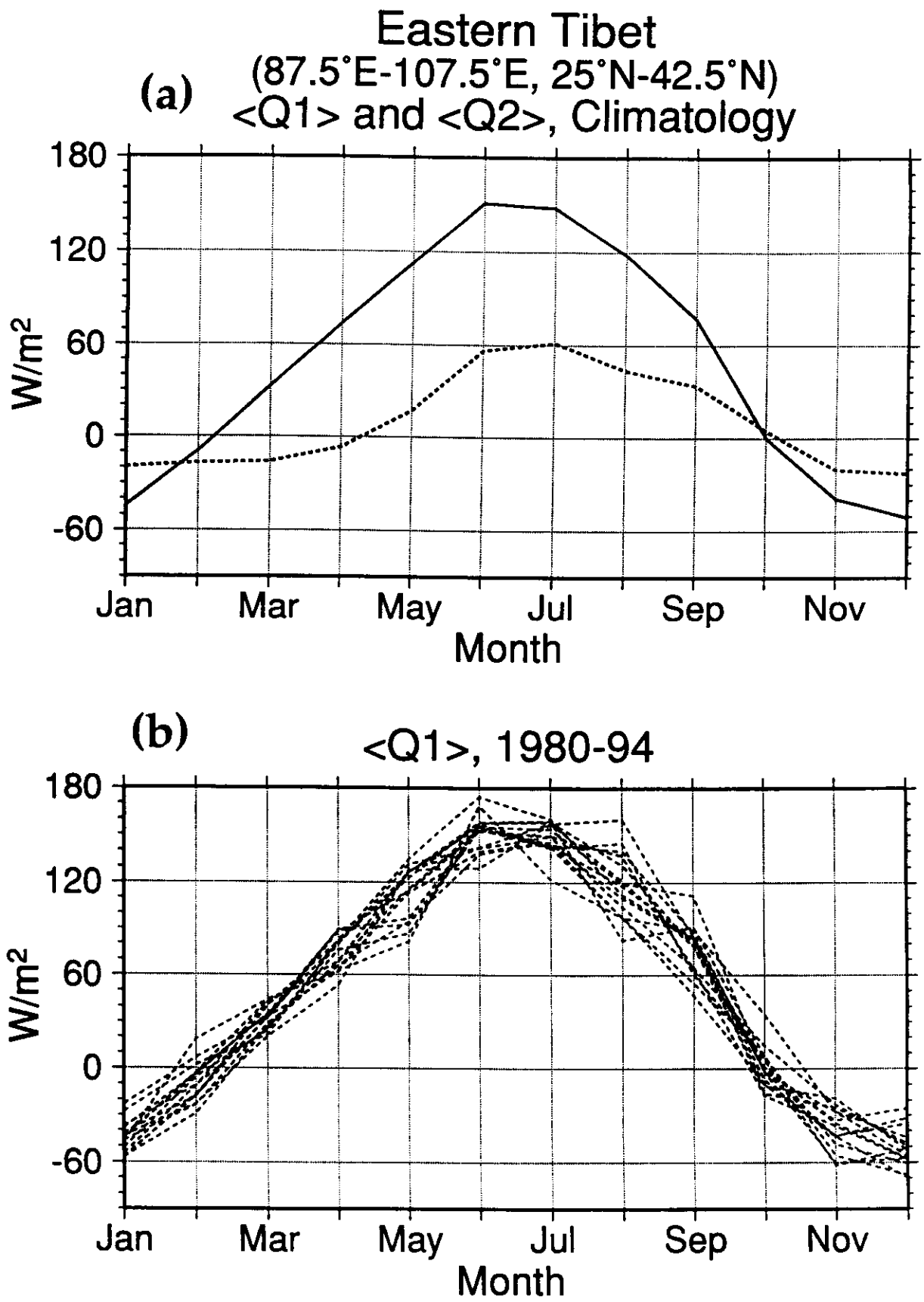

Fig. 16. As in Fig. 15 but for the eastern Tibetan Plateau.

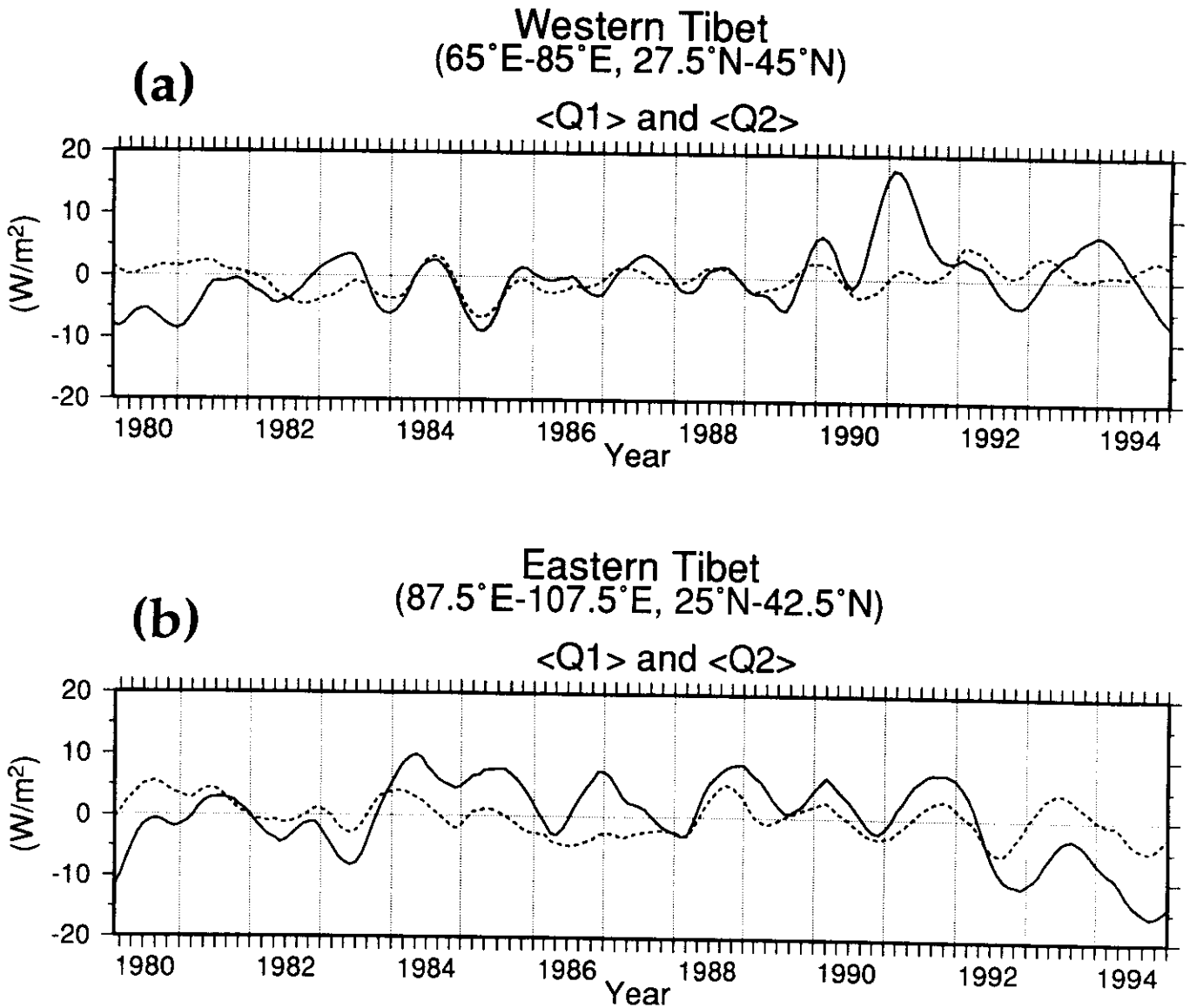

Fig. 17. Time series of monthly mean anomalies of $<Q_1>$ and $<Q_2>$ over (a) the western Tibetan Plateau, and (b) the eastern Tibetan Plateau.